TITLE

Protein structure analysis of the interactions between SARS-CoV-2 spike protein and the human ACE2 receptor: from conformational changes to novel neutralizing antibodies.

Authors

Ivan Mercurio[1*]; Vincenzo Tragni[2*]; Francesco Busco[1]; Anna De Grassi[1,3]; Ciro Leonardo Pierri[1,3§]

Affiliation:

[1]Laboratory of Biochemistry; Molecular and Structural Biology; Department of Biosciences, Biotechnologies, Biopharmaceutics; University of Bari; Via E. Orabona, 4; 70125 Bari, Italy

[2]Dipartimento di Scienze del Suolo, della Pianta e degli Alimenti, Università degli Studi di Bari Aldo Moro, Via Amendola 165/A, 70126 Bari, Italy

[3]BROWSer S.r.l. (https://browser-bioinf.com/) c/o Department of Biosciences, Biotechnologies, Biopharmaceutics; University "Aldo Moro" of Bari; Via E. Orabona, 4; 70126 Bari, Italy

Abbreviations: Severe acute respiratory syndrome, SARS; coronavirus CoV; receptor binding domain, RBD; angiotensin converting enzyme 2, ACE2; fragment antigen binding, FAB; Word Health Organizzation, WHO; complementary-determining regions, (CDR); SwissPDBViewer, SPDBV.

Keywords SARS-CoV-2; COVID-19; n-CoV19; coronavirus; spike; receptor binding domain; neutralizing antibodies; spike post-fusion conformation; ACE2; fold recognition tools; comparative modeling

*** These authors equally contributed**

§ Correspondence should be addressed to ciro.pierri@uniba.it; ciroleopierri1@gmail.com

ABSTRACT

The recent severe acute respiratory syndrome, known as Corona Virus Disease 2019 (COVID-19) has spread so much rapidly and severely to induce World Health Organization (WHO) to declare state of emergency over the new coronavirus SARS-CoV-2 pandemic. While several countries have chosen the almost complete lock-down for slowing down SARS-CoV-2 spread, scientific community is called to respond to the devastating outbreak by identifying new tools for diagnosis and treatment of the dangerous COVID-19. With this aim we performed an *in silico* comparative modeling analysis, which allows to gain new insights about the main conformational changes occurring in the SARS-CoV-2 spike protein, at the level of the receptor binding domain (RBD), along interactions with human cells angiotensin converting enzyme 2 (ACE2) receptor, that favour human cell invasion. Furthermore, our analysis provides i) an ideal pipeline to identify already characterized antibodies that might target SARS-CoV-2 spike RBD, for preventing interactions with the human ACE2, and ii) instructions for building new possible neutralizing antibodies, according to chemical/physical space restraints and complementary determining regions (CDR) mutagenesis of the identified existing antibodies. The proposed antibodies show *in silico* a high affinity for SARS-CoV-2 spike RBD and can be used as reference antibodies also for building new high affinity antibodies against present and future coronavirus able to invade human cells through interactions of their spike proteins with the human ACE2. More in general, our analysis provides indications for the set-up of the right biological molecular context for investigating spike RBD-ACE2 interactions for the development of new vaccines, diagnosis kits and other treatments based on the usage or the targeting of SARS-CoV-2 spike protein.

INTRODUCTION

Scientific community is called to respond to a pandemic of respiratory disease that has spread with impressive rate among people of all the world. The new coronavirus has been called SARS-CoV-2 and the related disease indicated as COVID-19. WHO reports that positive patients in the world are 1353361 with 79235 (April 9th, 2020) ascertained died people due to COVID-19 complications. It also appears that these numbers might be a smaller number of real cases due to our inability in quantifying rescued or asymptomatic people.

In order to limit death rate and SARS-CoV-2 spread, it needs to develop a vaccine and to identify new small molecules able to prevent or treat COVID-19 complications, as well as to prepare new quick diagnosis kits, able to quantify the real number of people exposed to SARS-CoV-2. Among the main actors of SARS-CoV-2 infection the SARS-CoV-2 spike proteins, RNA dependent RNA polymerases and proteases deserve to be mentioned. Indeed, RNA dependent RNA polymerase has become one of the main targets of a nucleoside analog antiviral drug, the remdesivir, already used for reducing complications due to Ebola, Dengue and MERS-CoV infections (1–6). At the same time viral protease inhibitors (7–10) are under investigation for their ability in preventing virus protein

(with specific reference to spike proteins) cleavage (11) leading to the fusion of virus proteins with host cell membranes. Also anti-inflammatory antibodies/drugs in combination with anticoagulant molecules are under investigation for limiting coagulopathies (12–15) and cytokine signaling impressively triggered by SARS-CoV-2 infection (16–20). Finally, the same SARS-CoV-2 spike protein has become the most investigated target due to its ability in forming interactions with the human ACE2 receptor, causing fusion events that make possible for the virus to penetrate host human cells (21–23).

The crucial role played by the spike protein is also due to the possibility to use the recombinant SARS-CoV-2 spike protein for triggering immune response, working as a vaccine, that may help in preventing and treating COVID-19, similarly to what proposed recently (24–26).

For clarifying SARS-CoV-2 infection mechanisms, several research groups have recently solved the crystallized structure of the entire SARS-CoV-2 spike protein (6vsb.pdb (21); 6vxx.pdb and 6vyb.pdb (22)), in pre-fusion conformation, and/or SARS-CoV-2 spike RBD domain in complex with the human ACE2 (6vw1.pdb; 6lzg.pdb).

In light of the available cited crystallized/cryo-em solved structures, here we propose a strategy for identifying/drawing new SARS-CoV-2 antibodies directed against the RBD of SARS-CoV-2 that could be used for contrasting SARS-CoV-2 infection, aiming to prevent pre-/post-fusion spike conformation interconversion, responsible for virus invasion, and to provide a molecular structural context for studying new diagnosis kits based on the interactions between our engineered antibodies and the human SARS-CoV-2 spike RBD.

MATERIALS AND METHODS

2.1. Crystal Structure Sampling Via Folding Recognition and multiple sequence alignments (MSA)

CoV-Spike and ACE2 homologus protein-crystallized structures were searched by using the folding recognition methods implemented in pGenThreader and i-Tasser according to our validated protocols (27–30).

The sequences of the retrieved 48 crystallized structures (with reference to those crystallized structures indicated with “Certain” or “High” confidence level in pGenThreader output) were aligned by using ClustalW (31) implemented in the Jalview package (32). The 3D coordinates from the 48 crystallized structures were superimposed for comparative purposes by using PyMOL (33) according to our validated protocols (29, 34).

Protein-protein and protein-ligand binding regions were highlighted by selecting residues within 4 Å at the protein-protein interface or from the investigated ligands, in the superimposed structures.

All the generated 3D all atom models were energetically minimized by using the Yasara Minimization server (35).

2.2. 3D atomic models preparation of SARS-CoV-2 Spike protein in post-fusion conformation and SARS-CoV-2 Spike-ACE2 interactions in pre-fusion conformations.

The 3D comparative model of SARS-CoV-2 spike trimer in post-fusion conformation was built by multi-template modeling by using Modeller (36). More in detail, the human SARS-CoV-2 spike protein sequence was aligned to the sequences of the available entire post fusion conformation of the murine coronavirus spike protein (6b3o, (37)) and the remaining available crystallized subdomains of other coronavirus spike proteins in post fusion conformations (5yl9.pdb (38); 1wyy.pdb (39) and 1wdf (40)). Sequences of the cited crystallized structure fragments were used as query sequences for sampling the corresponding entire spike monomer sequences, by reciprocal-blastp, to be aligned with sequences of the investigated structures for comparative purposes. The obtained MSA was used for driving the multi-template modeling.

Then a complex 3D model representing the pre-fusion spike trimer interacting with three ACE2 functional receptor units was built by superimposing the recently solved cryo-EM prefusion structure of SARS-CoV-2 spike trimer complex (6vsb.pdb, (21); 6vyb.pdb and 6vxx.pdb (22)), the SARS-CoV-2 spike RBD crystallized in complex with the human ACE2 (6vw1.pdb; 6lzg.pdb) the SARS-CoV-1 spike trimer interacting with one ACE2 functional receptor (conformations 1-3, 6acg.pdb, 6acj.pdb, 6ack.pdb, (41) and 6cs2.pdb, (42)), the SARS-CoV-1 spike-RBD crystallized in complex with the human ACE2 (2ajf.pdb, (43)).

For investigating pre-/post-fusion conformation interconversion we superimposed the pre-fusion available crystallized structures of SARS-CoV2 spike proteins and the generated 3D models about pre-fusion conformation of the spike trimer in complex with three ACE2 units, to the obtained 3D model of the post fusion conformation. All the generated 3D all atom models were energetically minimized by using the Yasara Minimization server (35)

2.3 Antibody 3D modeling and mutagenesis

Starting from the 3D atomic coordinates of the crystallized neutralizing antibodies m396 (2dd8.pdb(44)) and S230 (6nb7.pdb, (45)) directed against the SARS-CoV-1 spike RBD domain, we modelled the interactions of m396 and S230 (6nb7.pdb, (45)) with SARS-CoV-2 spike RBD domain, by superimposing the fragment antigen based (FAB) portions of m396 (2dd8.pdb (44)) and S230 (6nb7.pdb, (45) (both complexed with SARS-CoV-1 RBD) with the SARS-CoV-2 spike RBD domain, complexed with ACE2 (6vw1.pdb), by using PyMOL.

For creating a more specific antibody directed against SARS-CoV-2 spike RBD, we replaced residues of the CDR regions of the m396 crystallized FAB portion with residues that may complement and fulfill better the SARS-CoV-2 RBD surface. Mutagenesis analyses and modeling of the incomplete residues within the crystallized structures were performed by using SPDBV (46) and/or PyMOL (47).

The proposed complete IgG chimeric antibodies were obtained by superimposing the above cited m396 and the resulting engineered FAB portions, in complex with SARS-CoV-1/2 RBD, to the 3D atomic model of a crystallized IgG, available on the PDB (1igt.pdb, (48)) by using SPDBV and PyMOL, according to our validated protocols (29, 30, 49), that allow to model missing residues, solving clashes and breaks in the backbone.

Each glycosylation ladder coming from the crystal structures here investigated (1igt.pdb; 2dd8.pdb; 6nb7.pdb) was alternatively retained within the generated structural models.

After superimposition operations, allowing backbone connections, we renumbered all the atoms and the residues present in the resulting final pdb file, by using an in-house developed Perl script. The obtained final models were examined in VMD, PyMOL, and SPDBV according to our protocols (30, 49). All the generated 3D all atom models were energetically minimized by using the Yasara Minimization server (35).

2.4. Energy calculations

The FoldX AnalyseComplex assay, was performed to determine the interaction energy between the four generated antibodies and the RBD domains of SARS-CoV-1/2 spike proteins, but also for determining the interaction energy between ACE2 and the interacting spike RBDs for comparative purposes.

The way the FoldX AnalyseComplex operates is by unfolding the selected targets and determining the stability of the remaining molecules and then subtracting the sum of the individual energies from the global energy. More negative energies indicate a better binding. Positive energies indicate no binding (50, 51). The energy calculated for the crystallized m396-SARS-CoV-1 RBD protein complex was used as a reference value.

RESULTS

3.1. Modelling of the SARS-CoV-2 spike protein in post-fusion conformation.

The main event that allows virus envelop fusion with the host human cell plasma membrane concerns a conformational change occurring at the SARS-CoV-2 spike protein that converts from pre-fusion conformation to post-fusion conformation after interactions with ACE2 and spike protein cleavage. While SARS-CoV-2 spike protein trimer has been resolved by cryo-em (6vsb.pdb (21); 6vxx.pdb and 6vyb.pdb (22)), the post-fusion conformation is not available, yet. According to (11) Coutard et al., protein cleavage at site S1/S2 and S2' produces the division of the spike protein in two subdomains, i.e. the N-ter S-I ectodomain (containing the RBD interacting with ACE2) and the C-ter S-II membrane anchored subdomain, forming the SARS-CoV-2 spike protein in post fusion

conformation, able to trigger the fusion of the viral envelope with host cell plasma membrane determining host cell invasion.

For modelling 3D post-fusion conformation of SARS-CoV-2 spike protein we searched for SARS-CoV-2 spike protein homologous structures and found 48 crystallized structures that included poses of the whole SARS-CoV-2 spike proteins or about protein domains of SARS-CoV-2 spike proteins in complex with protein interactors (i.e. ACE2), several pre-fusion conformations of other coronavirus spike proteins, one coronavirus spike protein in post-fusion conformation and three further protein subdomains about spike proteins in post fusion conformation (Supp. Tab. 1).

Thus, we built a MSA by aligning the sequence of the human SARS-CoV-2 spike protein, the sequence of the available whole post fusion conformation of the murine coronavirus spike protein (6b3o, (37)), sequences of the remaining crystallized subdomains of other coronavirus spike proteins in post fusion conformations (5yl9.pdb (38); 1wyy.pdb (39) and 1wdf (40)), together with their complete counterpart sequences sampled by reciprocal-blastp (Fig. 1).

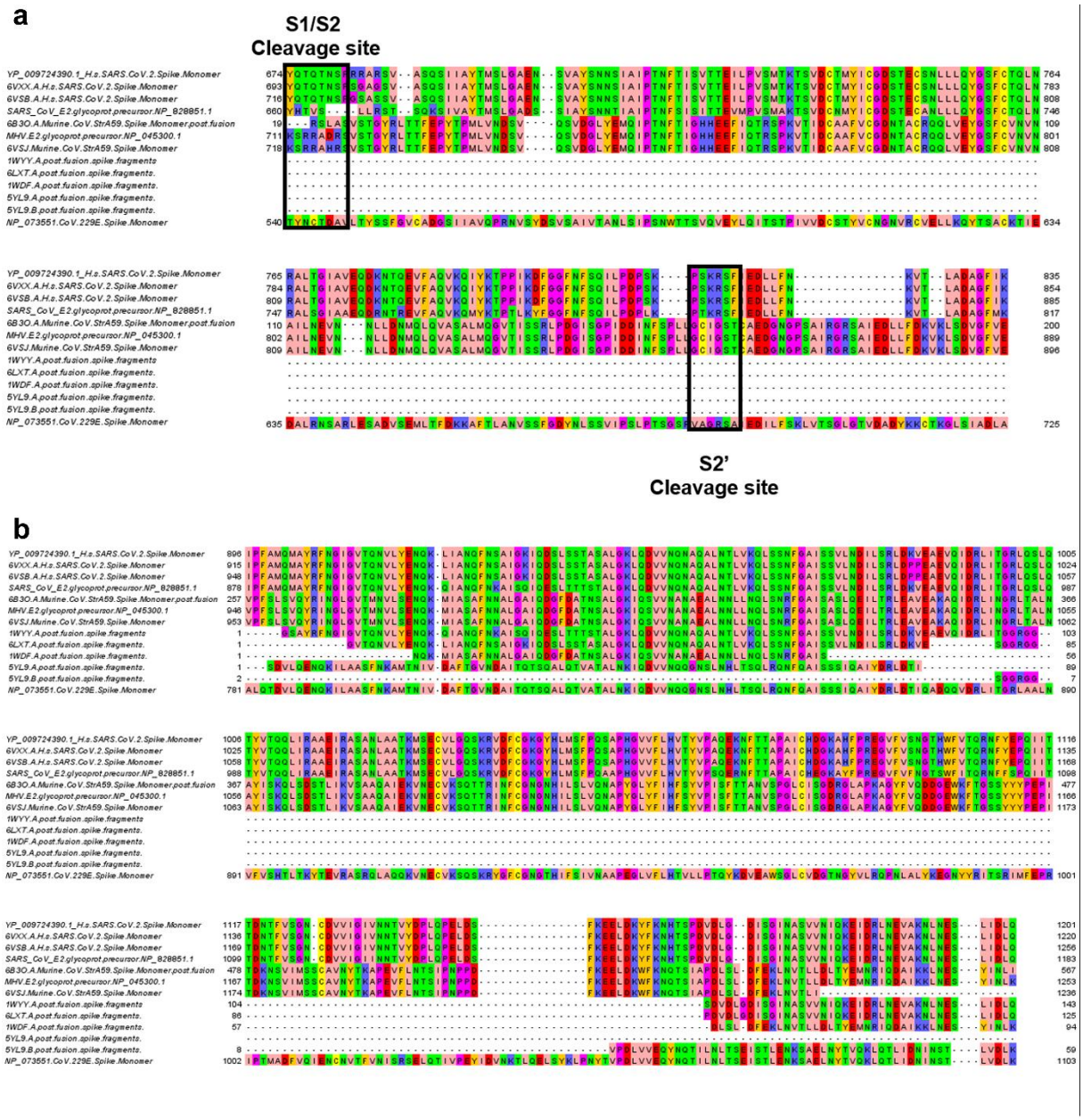

Fig. 1 Extract of the MSA of SARS-CoV-2 spike protein monomer with the sequences of crystallized structures of the spike whole protein or protein fragments observed in the post-fusion conformation from other coronavirus, resulting from sequence cleavage. Panel a. Black boxes indicate the position of cleavage sites. In panel "a" it is reported the 6b3o.pdb based sequence-structure alignment used for modeling the first portion of SARS-CoV-2 spike protein in post fusion conformation (amino acids S704-771A, YP_009724390.1 residues numbering). In panel "b" it is reported the 6b3o.pdb based sequence-structure alignment used for modeling the second portion of SARS-CoV-2 spike protein in post fusion conformation (amino acids 922-1147, YP_009724390.1 residues numbering).

In the provided MSA (Fig. 1) it is possible to observe the conserved S1/S2 and S2' cleavage sites, according to (11) and the sequence of the C-terminal domain resulting from the cleavage.

Starting from the cited multi-template sequence alignment and according to our validated protocols about multi-template 3D modeling (30, 36), we built the 3D model of a monomer of SARS-CoV-2 spike protein in post fusion conformation (Fig. 2). The modelled SARS-CoV-2 spike post-fusion conformation consists of residues 704-771 and 922-1147, YP_009724390.1 residues numbering, resulting from protein cleavage (11) and also the only protein fragments with a solved structure in

6b3o.pdb aligned (aminoacids 741-807 and 972-1248, NP_045300.1/6b3o.pdb residues numbering) counterpart (37).

The trimer of the SARS-CoV-2 spike protein in post fusion conformation was obtained by duplicating two times the obtained monomer and superimposing the three SARS-CoV-2 spike protein monomers on the three SARS-CoV-1 spike protein monomers reported in 6b3o.pdb (Fig. 2). The 3D comparative model of SARS-CoV-2 spike protein trimer built by multi-template comparative modeling showed an RMSD lower than 0.5 Å with the murine coronavirus spike protein in post-fusion conformation (6b3o.pdb). The resulting model (Fig. 2) appeared elongated and narrow, according to what observed in fragments of the spike proteins crystallized in post-fusion conformations, whose sequences are reported in Fig. 1 and whose PDB_ID are listed in Supp. Tab. 1.

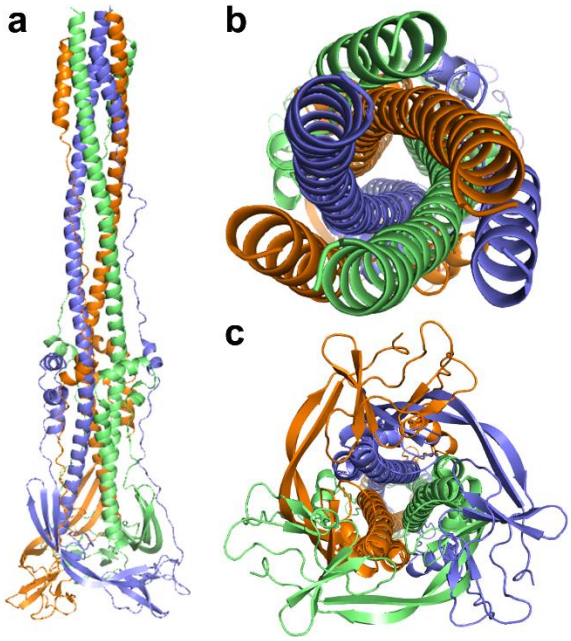

Fig. 2. SARS-CoV-2 spike protein (S-II domain) 3D model in post fusion conformation. Lateral view (panel a), top view (panel b) e bottom view (panel c) of the SARS-CoV-2 spike protein trimer 3D comparative model, reported in cartoon colored representation.

3.2. Modelling of the interactions between the SARS-CoV-2 spike protein and the human ACE2 along pre-/post-fusion conformation interconversion.

Among the sampled crystallized structures, it was possible to observe three PDB_ID about the entire SARS-CoV-2 spike proteins and two about SARS-CoV-2 spike RBD protein interacting with the human ACE2 (Supp. Tab. 1). Furthermore, it was possible to highlight several crystallized structures about SARS-CoV-1 and MERS-CoV spike proteins as single proteins or in complex with their receptors or dedicated antibodies (Supp. Tab. 1). Notably, among the sampled structures, also the four entries used for building the 3D comparative model of the post-fusion conformation, were sampled (Supp. Tab. 1).

For modeling main interactions occurring between SARS-CoV-2 spike proteins and ACE2, thanks to the high percentage of identical residues shared by spike RBD from several CoV strains (Fig. 3), it was possible to structurally align three objects consisting of the human ACE2-SARS-CoV-1 spike-RBD protein complex (2ajf.pdb) to the human ACE2-SARS-CoV-2 spike-RBD protein complex (6vw1.pdb, 6lzg.pdb) and the SARS-CoV-2 spike protein trimer (6vsb.pdb; 6vxx.pdb; 6vyb.pdb). More in detail, the superimposition performed by using PyMol was leaded by the structural alignment of the RBD of ACE2-SARS-CoV1 (2ajf.pdb) and ACE-2-SARS-CoV-2 (6vw1.pdb, 6lzg.pdb) spike proteins (Fig. 4), followed by the structure alignment with SARS-CoV-2 spike protein trimer (6vsb.pdb; 6vxx.pdb; 6vyb.pdb). Notably, we obtained an efficient superimposition of the two RBD domains (RMSD lower than 0.5 Å) of the human SARS-CoV-1 and SARS-CoV-2 spike proteins also due to their high percentage of identical residues (> 75%).

It was possible to superimpose the crystallized SARS-CoV-2 spike protein in pre-fusion conformation and the modelled SARS-CoV-2 spike protein trimers in post-fusion conformation for showing the deep conformational changes occurring along conformation interconversion (Fig. 4). Apparently, the post-fusion conformation appears to be elongated and narrower than the pre-fusion conformation. The top portion of the post-fusion conformation locates beyond ACE2 receptors (Fig. 4), known for being anchored to plasma membrane and involved in internalization events (7, 41, 44, 45, 52).

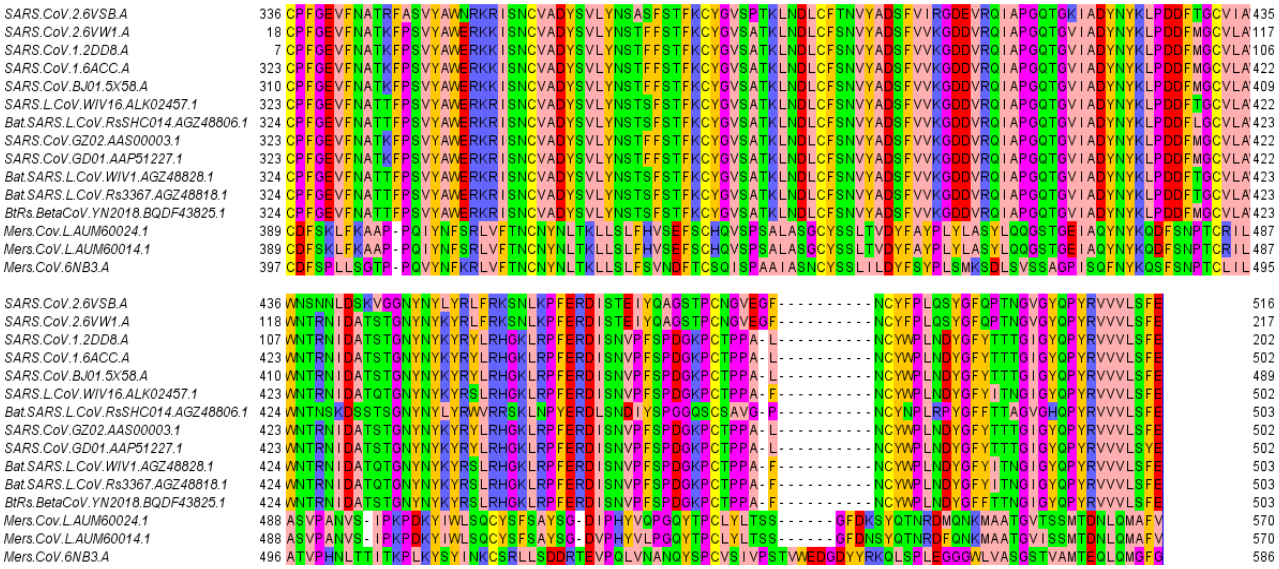

Fig. 3 Multiple sequence alignment of RBDs from 11 SARS-CoV and 3 MERS-CoV strains. The reported residues numbering refers to the indicated sequences sampled by blastp or to the indicated crystallized structure sequences.

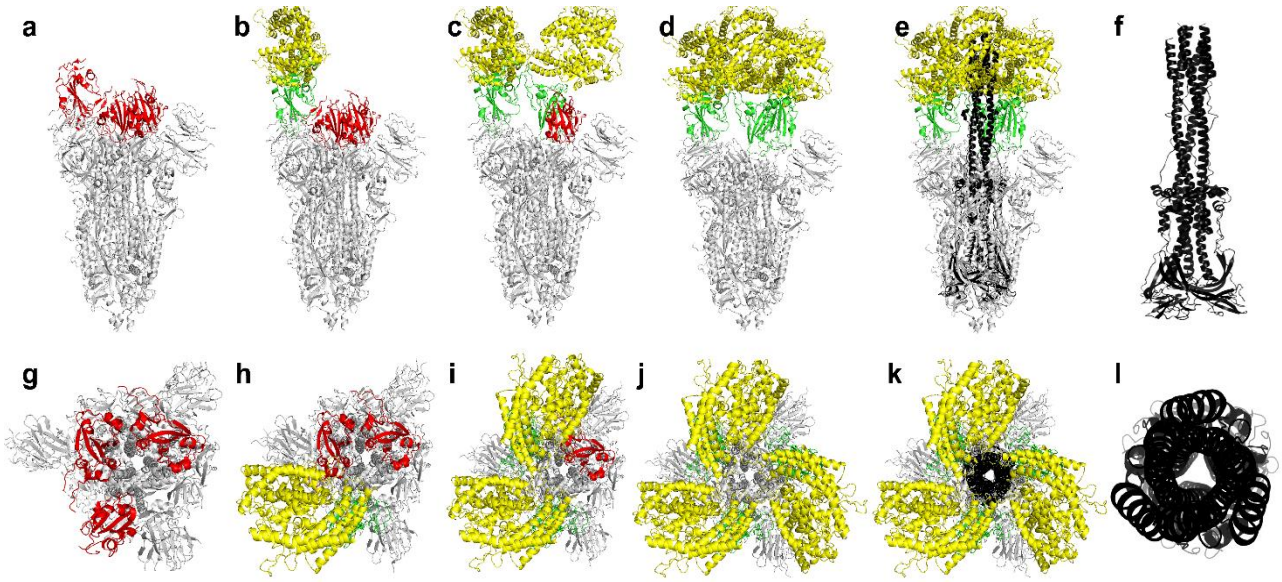

Fig. 4 Side view (panels a-f) and top view (panes g-l) of H. sapiens SARS-CoV-2 spike protein interacting with 3 units of the human ACE2 N-terminal domain (panels a-e; g-k). SARS-CoV-2 spike protein trimer (6vsb.pdb) is reported in white cartoon representation with the 3 spike receptor binding domains reported in red (in the closed pre-fusion state) or green (in the open pre-fusion state) cartoon. The open pre-fusion state allows establishing pre-invasion interactions with ACE2 N-terminal domain. SARS-CoV-2 spike protein trimer C-terminal domain, resulting from protein cleavage that triggers the post-fusion conformation, is reported in black cartoon representation in panel f (lateral view) and l (top view).

3.3. SARS-CoV-1 and SARS-CoV-2 RBD residues involved in direct interactions with ACE2

From the available crystallized structures and from the obtained 3D structure models it was possible to highlight SARS-CoV-1 spike RBD (2ajf.pdb) and SARS-CoV-2 spike RBD residues (6) involved in the binding of the human ACE2 (Fig. 5 and Supp. Tab. 1). Notably, ion pair interactions observed between SARS-CoV-1 spike RBD and the human ACE2 are also observed between SARS-CoV-2 spike RBD and the human ACE2. The reported data represents an updated/integrated analysis of a similar ones reported in (53), in light of the recently deposited SARS-CoV-2 spike RBD in complex with the human ACE2 (6vw1.pdb).

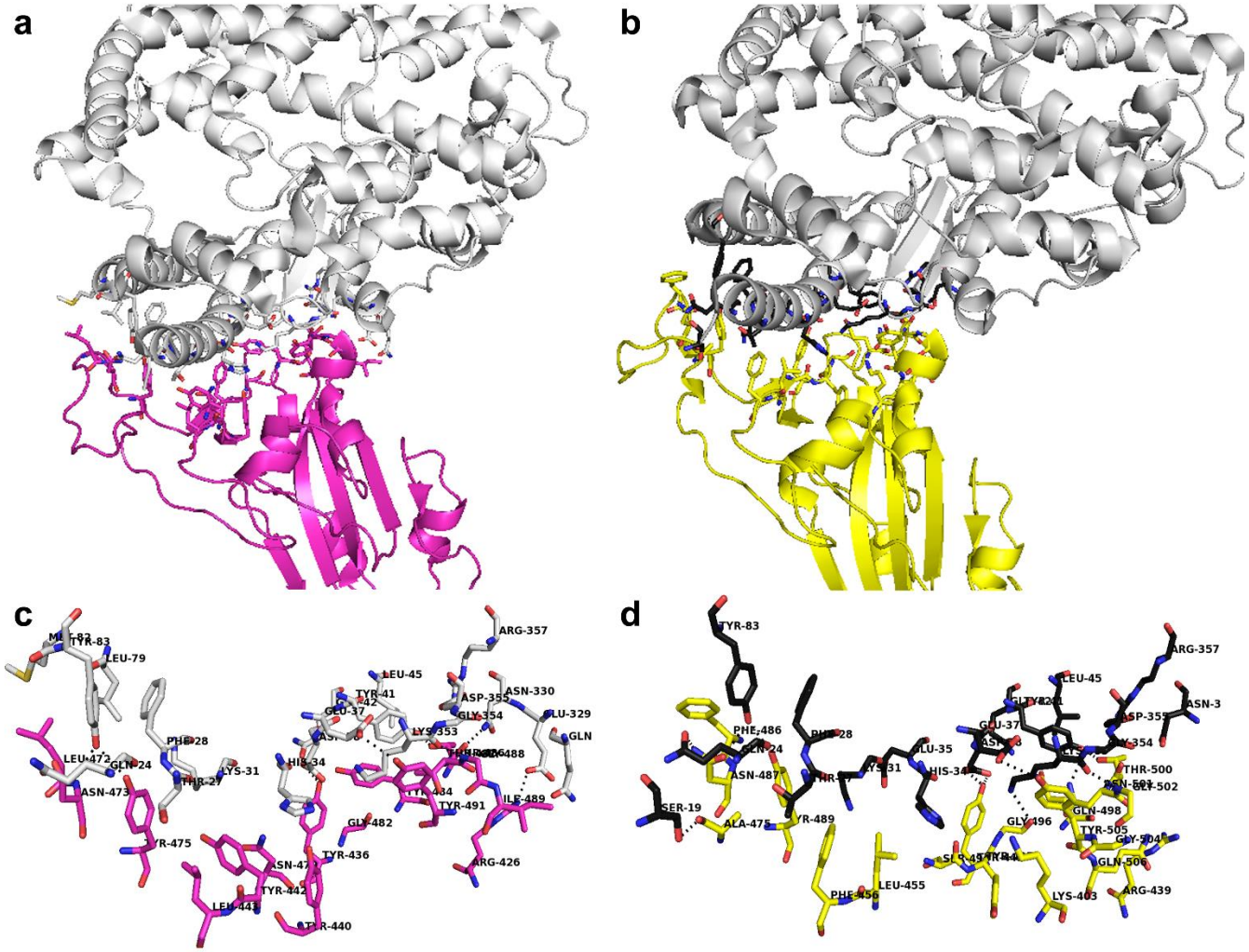

Fig. 5. SARS-CoV-1 and SARS-CoV-2 RBD residues involved in direct interactions with ACE2. H. sapiens ACE2 is reported in white cartoon representation. SARS-CoV-1 RBD is reported in magenta cartoon representation, whereas SARS-CoV-2 RBD is reported in yellow cartoon representation. Panel a, c. Residues involved in polar interactions between SARS-CoV-1 RBD (magenta sticks) and ACE2 (white sticks). Panels b, d. Residues involved in polar interactions between SARS-CoV-2 RBD (yellow sticks) and ACE2 (black sticks). Polars interactions are represented by black dashed lines in the exploded views reported in panels c and d.

ACE2.interacting.residues.with SARS.CoV.1.RBD (2ajf.pd)b		**ACE2.interacting.residues.with SARS.CoV.2.RBD (6vw1.pdb)**	
ACE2 (chain A)	**SARS.CoV.1.RBD (chain E)**	**ACE2 (Chain B)**	**SARS.CoV.2.RBD (Chain F)**
		S19	**A475**
Q24	**N473**	**Q24**	**N487**
Y83	**Y475**	**Y83**	**Y489**
		E37	**Y505**
D38	**Y436**	**D38**	**Y449**
Q42			
Y41	**T486**	**Y41**	**T500**
N330			**N501**
K353	**T487**	**K353**	**G496**
		G354	**G502**
E329	**R426**		
T27	L45	T27	K403
F28	Y83	F28	R439
K31	Y440	K31	L455
H34	Y442	H34	F456
E37	L443	E35	F486
L45	L472	Q42	S494
L79	N479	L45	Y495
M82	G482	N330	Q498
Q325	Y484	D355	G504
N330	G488	R357	Q506
G354	I489		
D355	Y491		
R357			

Tab. 1 List of SARS.CoV.1 and SARS.CoV2 RBD residues and of ACE2. Bold black residues delimited by borders indicate a pair or a cluster of residues involved in polar inter-protein interactions. Normal black residues indicate residues at the Spike-RBD.vs.ACE2 protein interface distant less than 4 Å. The longest chains were chosen within those crystallized structures with multiple chains, for highlighting the listed interacting residues.

3.4. Comparative analysis of existing SARS.CoV.1. Spike RBD directed neutralizing antibodies and interaction predictions with SARS.CoV.2 Spike RBD.

RBD from SARS-CoV-1 was crystallized in complex with the FAB domain of two different antibodies, namely m396 (2dd8.pdb, (44)) and S230 (6nb7.pdb, (45)). Both of them show high affinity for SARS-CoV-1 spike RBD, being able to block attachment to ACE2 (44, 45). Nevertheless, they show different peculiarities in their mechanism of action.

Indeed, S230 after binding RBD, similarly to ACE2, is able to trigger the SARS-CoV spike transition to the post-fusion conformation and it is not clarified yet, if virus-cell fusion may be triggered by S230 also when S230-RBD interactions occurs close to the surface of the cells target of the SARS-CoV-1 (45). At variance with S230, m396 antibody appears to be able to prevent SARS-CoV-1 spike-ACE2 interactions and SARS-CoV-1 spike pre-/post-fusion conformation transition, neutralizing virus attack (44).

Thanks to the high percentage of identical residues (> 75 %) between SARS-CoV-1 and SARS-CoV-2 spike RBD domains and to their highly similar tertiary structure, as observed from the RMSD of 0.5 Å between the coordinates of RBDs from SARS-CoV-1 (6nb7.pdb, (45) and 2dd8.pdb, (44)) and SARS-CoV-2 (6vw1.pdb (54) and 6vsb.pdb, (21)) spike proteins, it was possible to evaluate interactions between m396 and SARS-CoV-2 spike RBD and to propose a sequence/structure of an ideal FAB m396-based chimeric antibody for targeting SARS-CoV-2 spike RBD domain, preventing fusion events with ACE2 and thus the following infection.

With this aim, we firstly highlighted the different RBD portions bound to the known antibodies. Then, we superimposed SARS-CoV-1 RBD to SARS-CoV-2 RBD for highlighting differences in residues involved in direct interactions with m396 CDR regions and with S230 CDR regions (Fig. 6 and Tab. 1).

SARS.CoV.1.RBD (6nb7.pdb) crystallized residues within 4 Å from S230 (6nb7a)	**S230ab (6nb7a) residues within 4 Å from SARS.CoV.1.RBD (6nb7.pdb)**	**SARS.CoV.2.RBD (6vw1.pdb) predicted residues within 4Å from S230 (6nb7a)**	**S230ab (6nb7a) predicted residues within 4Å from SARS.CoV.2.RBD (6vw1.pdb)**	**SARS.CoV.1.RBD (2d88.pdb) crystallized residues within 4 Å from md396**	**m396.ab (2d88) residues within 4 Å SARS.CoV.1.RBD (6nb7.pdb)**	**SARS.CoV.2.RBD (6vw1.pdb) predicted residues within 4 Å from m396 (2d88)**	**m396.ab (2d88) residues within 4 Å SARS.CoV.2.RBD (6vw1.pdb)**
T402		T415		T359	N27.L	T372	G29.L
G403	Y31.L	V417	Y31.L		I28.L	F374	S30.L
D407	S32.L	D420	S32.L	S362	K31.L	S375	
Y408		Y421		T363	S32.L	T376	W91.L
	zz			K365	H34.L		S93.L
R441				K390		**K403**	D95A.L
Y442		**L455**		G391	N66.L	G404	Y96.L
L443		**F456**		D392	G68.L	D405	
R444		R457		R395	Q89.L	R408	S31.H
H445	W99.L	K458	W99.L	**R426**	V90.L	**R439**	Y32.H
G446	P100.L	S459	P100.L	Y436	D92.L		T33.H
K447		N460		G482	S95.L	**G496**	
				Y484	Y96.L	**Q498**	T52.H
F460	R56.H	Y473		T485	V97.L	P499	I53.H
S461	N57.H	Q474	N57.H	**T486**		**T500**	L54.H
P462	K58.H	**A475**	K58.H	**T487**	S30.H	**N501**	I56.H
D463	F59.H	G476	F59.H	G488	I34.H	**G502**	A57.H
G464	Y60.H	S477	Y60.H	I489	S35.H	V503	N58.H
K465			K65.H	G490	W47.H	**G504**	V97.H
L472	R104.H	F486	G66.H	Y491	G49.H	**Y505**	G99.H
N473	Y106.H	**N487**		Q492	P52A.H	**Q506**	
Y475	F107.H	**Y489**	R104.H	Y494	G55.H	Y508	
	P108.H		Y106.H		Y59.H		
	H109.H		F107.H		I69.H		
	F111.H				T70.H		
			H109.H		T71.H		
					A93.H		
					R94.H		
					T96.H		
					M98.H		
					G100.H		
					M100A.H		

Tab. 2 List of SARS-CoV-1/2 RBD residues within 4 Å from S230/m396 antibody residues. Bold residues indicate SARS.CoV.1 residues interacting alternatively with both ACE2 and/or m396/S230 in the crystallized available structures. Distance range below 4 Å. Bold underlined residues indicate SARS.CoV.2 residues interacting with ACE2 and predicted to interact with m396 in a distance range below 4 Å

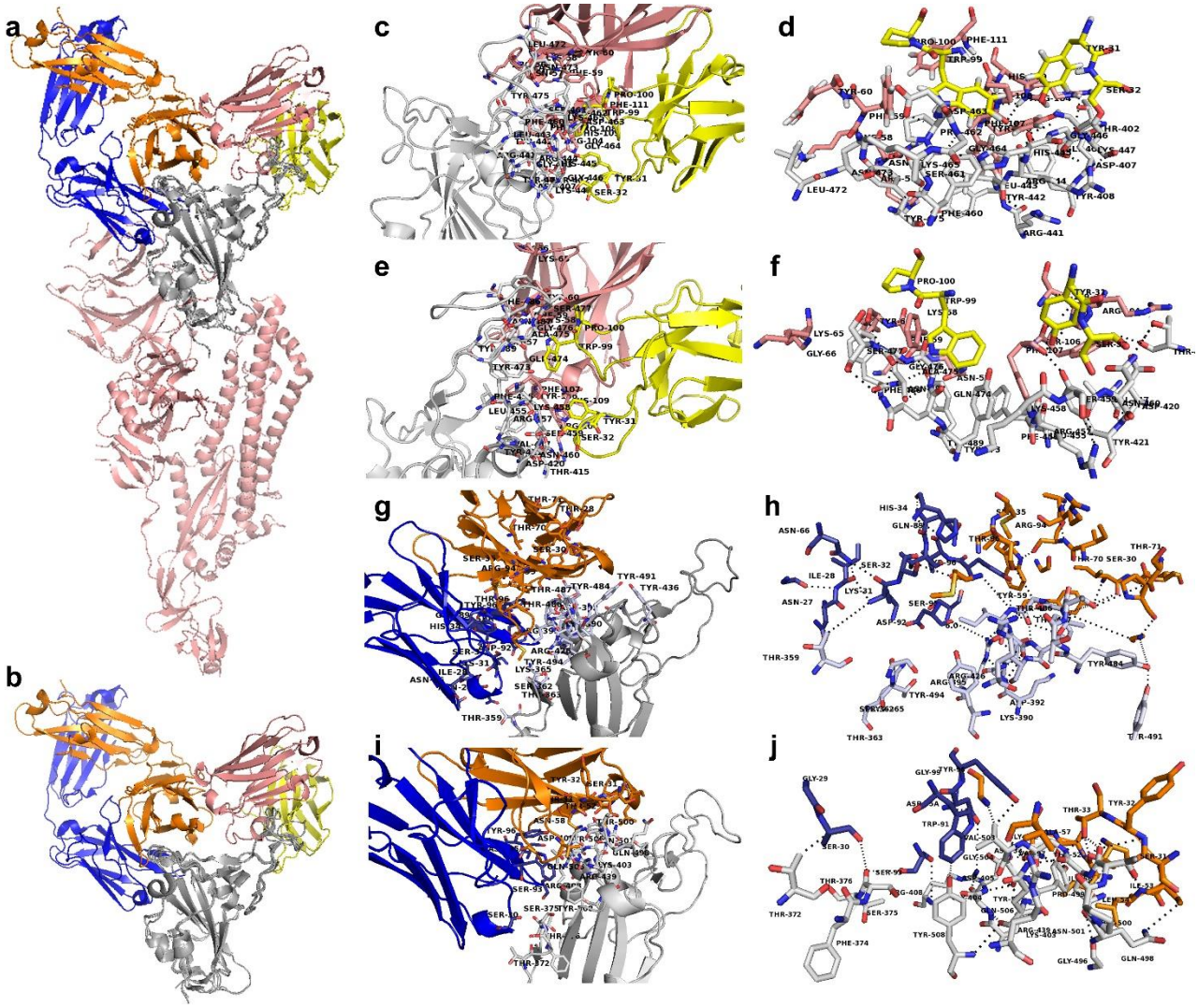

Fig. 6 SARS.CoV.1 Spike and SARS.CoV.2 Spike monomers in pre-fusion conformation interacting with SARS.CoV.1 Spike RBD selective antibodies S230 (6nb7.pdb) and m396 (2dd8.pdb). Panel a. Superimposition of the tertiary structure of SARS.CoV.1 (6nb7.pdb) and SARS.CoV.2 (6vsb.pdb) spike protein monomers reported in pink cartoon representation. SARS.CoV.1 and SARS.CoV.2 RBDs are reported in grey cartoon representation. S230 FAB ab portion (6nb7.pdb) is reported in yellow (light chain) and pink (heavy chain) cartoon representation. m396 FAB ab portion (2dd8.pdb) is reported in orange (light chain) and blue (heavy chain) cartoon representation. Panel b. zoomed view of the superimposition of SARS.CoV.1 Spike and SARS.CoV.2 Spike RBD domains interacting with S230 and m396 FAB antibodies (see Panel a. for colors). Panel c-d. Super zoomed and rotated views of the crystallized SARS.CoV.1 Spike RBD residues interacting with S230 ab. Panel e-f. Super zoomed and rotated views of SARS.CoV.2 Spike RBD predicted residues interacting with S230 ab. Panel g-h. Super zoomed and rotated views of the crystallized SARS.CoV.1 Spike RBD residues interacting with m396 ab. Panel i-j. Super zoomed and rotated views of SARS.CoV.2 Spike RBD predicted residues interacting with m396 ab. Panels c-j Residues at the RBD – ab interface in the 3.5- 4 Å distance range are reported in sticks representation. White sticks indicate RBD residues; orange and blue sticks indicate m396 ab residues, yellow and pink sticks indicate S230 ab residues.

3.5 SARS.CoV.2 Spike RBD directed neutralizing antibody engineering

Due to the uncertain data concerning fusion events and mechanism of action of S230 antibody, we built a new SARS-CoV-1/2 RBD directed antibody starting from the analysis of monomer-monomer interface interactions observed between the m396 antibody crystallized in complex with SARS-CoV-1 RBD (44), superimposed to SARS-CoV-1 spike RBD / ACE2 complex (2ajf.pdb), and by comparing them with monomer-monomer interface interactions observed between the modelled m396 antibody in complex with SARS-CoV-2 RBD, superimposed to SARS-CoV-2 RBD/ACE2 (6vw1.pdb; 6lzg.pdb) protein complex (Fig. 7).

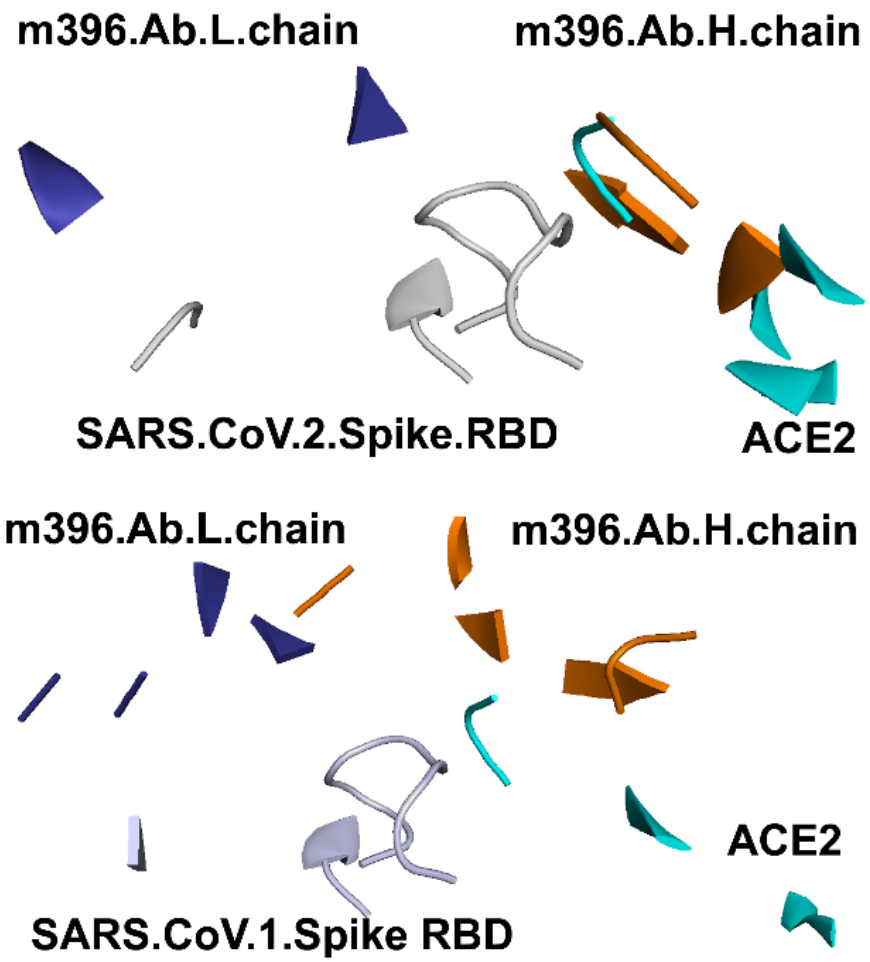

Fig. 7. Molecular framework of the investigated proteins hosting SARS-CoV-spike RBDs, light and heavy chain of the m396 antibody and the human ACE2, simultaneously. The shown spike RBD, ACE2 and m396 protein portions are those in a reciprocal distance range of 4 Å. Upper panel: Superimposition of the crystallized SARS-CoV-1 spike RBD (white cartoon representation) in complex with m396 antibody (2d88.pdb, orange and blue cartoon) and ACE2 (2ajf.pdb, cyan cartoon). Bottom panel: superimposition of SARS-CoV-2 spike RBDs (from 6vw1.pdb, white cartoon representation), ACE2 from 6vw1.pdb (cyan cartoon) and m396 from 2d88.pdb (orange and blue cartoon).

Then, we highlighted m396 CDR residues (Tab. 2) for replacing them aiming to increase m392 affinity versus SARS-CoV-1/2 spike RBDs. Residues to be mutated/replaced were chosen according

to space-restraints and chemical needs for better complementing SARS-CoV-1/2 spike RBD surface, based on the available SARS-CoV-1/2 RBD structures in complex with ACE2, aiming to produce something that resembled ACE2 surface (Tab. 1-2). Some of the proposed mutated residues (Tab. 3) are surely allowed because already observed at the corresponding sites of other known antibodies, according to Chotia/Kabat rules (http://www.bioinf.org.uk/abs/chothia.html; (55)). Residues replacement was directly performed in the newly generated 3D model hosting the interacting m396-SARS-CoV-2 spike RBD. Similarly, a complex of the modified m396 antibody interacting with SARS-CoV-1 RBD was also created. All m396 CDR mutated residues are reported in Tab. 3. Furthermore, mutated residues within m396 CDR interacting with SARS-CoV-2 spike RBD residues can be observed in Fig. 8.

	Mutations based on space restraints needs*	**Allowed variants#**		**Mutations based on space restraints needs***	**Allowed variants#**
CDR-L1			**CDR-H1**		
24-GGNNIGSKSVH-34	S30R; K31R	G25A; N26S; I28N/S/D/E; G29I/V; S32Y	26-GGTFSSYTIS-35	S31K; T33E	
CDR-L2			**CDR-H2**		
50-DDSDRPS-56		D51A/T/G/V	50-GITPILGIANYAQKFQG-66	L55D; I57Y;	T52D/L/N/S/Y; I54A/G/Y/S/K/T/N; L55N/S/T/K/D/G; I57Y/R/E/D/G/V/S/A
CDR-L3			**CDR-H3**		
89-QVWDSSSDYV-98	S94E; S95R	V90Q; D92S; Y97I; V98T	99-DTVMGGMDV-17	V101K; G103L	

Tab. 3. List of CDR L/H residues detectable in m396 antibody according to Chotia/Kabat classification. The investigated (*) built variants (column "Mutations based on space restraints needs") and (#) known mutations (column "Allowed variants") according to Chotia/Kabat rules are also reported for comparative purposes.

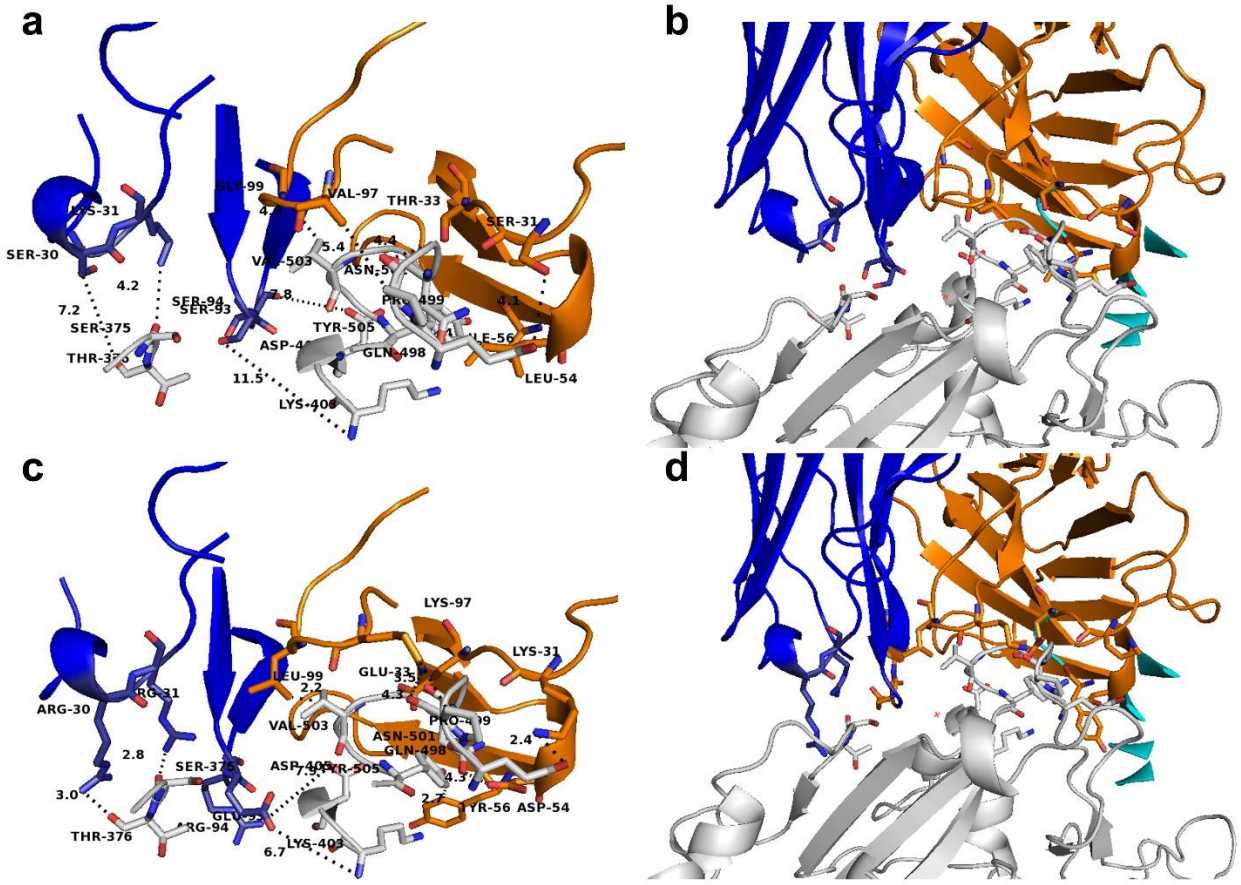

Fig. 8. m396 neutralizing antibody, native and engineered, in complex with SARS-CoV-2 spike RBD. Panels a-b: exploded view and perspective view of native m396 neutralizing antibody (in orange blue cartoon) in complex with SARS-CoV-2 spike RBD (in white cartoon representation). Residues at the m396/RBD interface in a distance range withni 4 are indicated by white sticks (RBD), orange sticks (m396 CDR-H residues) and blue sticks (m396 CDR-L residues). Panels c-d: exploded view and perspective view of the engineered m396 predicted neutralizing antibody (in orange blue cartoon) in complex with SARS-CoV-2 spike RBD (in white cartoon representation). Residues at the engineered m396/RBD interface in a distance range within 4 Å are indicated by white sticks (RBD), orange sticks (engineered m396 CDR-H residues) and blue sticks (engieered m396 CDR-L residues).

The engineered FAB portions were thus aligned and superimposed on the FAB portion of a crystallized IgG (1igt.pdb, (48)). The sequence of the chimeric antibodies can be observed in Supp. Fig. 1, whereas their complete structure can be observed in Supp. Fig. 2.

3.6 Free energy calculation

The interaction energies calculated between the SARS-CoV-2 spike RBD domain and m396 native antibody FAB portion gives a negative value (Tab. 4), confirming that there might be a binding interaction between m396 native antibody FAB portion and SARS-CoV-2 spike RBD. This result is encouraging, also due to the indirect validation obtained by getting similar interaction energies for the crystallized SARS-CoV-1 RBD in complex with m396 (2d88.pdb) and for SARS-CoV-1 and SARS-CoV-2 spike RBD domains crystallized in complex with ACE2 (2ajf.pdb and 6vw1.pdb, respectively) (Tab. 4). Furthermore, a strong interaction (in terms of interaction energies calculated by FoldX Analyse complex assay) is also predicted between SARS-CoV-2 spike RBD (but also

SARS-CoV-1 spike RBD) and the modified m396 antibody (see Tab. 4), suggesting that the engineered m396 might be more efficient than the native m396 in binding the SARS-CoV-2 (more than SARS-CoV-1) spike RBD.

Interaction energies (FoldX AnalyseComplex)	**Crystallized Structures**	**Crystallized Structures**	**Crystallized Structures**	**PreMin 3D model**	**PostMin 3D model**	**PreMin 3D model**	**PostMin 3D model**	**PreMin 3D model**	**PostMin 3D model**
Evaluated parameters	**ACE2.RBD1 (2ajf)**	**ACE2.RBD2 (6vw1)**	**m396.orig.RBD1 (2dd8)**	**m396.orig.RBD2**	**m396.orig.RBD2**	**m396.mod.RBD1**	**m396.mod.RBD1**	**m396.mod.RBD2**	**m396.mod.RBD2**
Group1 (RBD.PDB.Chain)	E	F	S	F	F	S	S	F	F
Group2 (PDB.Chain)	A	B	HL	HL	HL	HL	HL	HL	HL
IntraclashesGroup1	152,996	34,6023	60,6311	34,7844	10,4901	60,5936	12,6289	34,7081	5,43578
IntraclashesGroup2	42,6681	76,8707	115,607	115,618	26,1664	121,985	26,2721	121,981	22,2216
InteractionEnergy(Kcal/mol)	**-8,27337**	**-4,99501**	**-6,38302**	29,781	**-5,94391**	83,0763	**-5,79798**	97,994	**-6,11027**
BackboneHbond	-1,64493	-2,58671	-2,02004	-1,47563	-3,14458	-1,55689	-2,61412	-1,35295	-6,45205
SidechainHbond	-3,65689	-7,82596	-6,8445	-2,22654	-5,14948	-6,16783	-7,27162	-1,85715	-9,05615
Vander Waals	-12,8528	-14,6465	-14,78	-13,706	-14,2857	-19,8527	-18,3596	-18,7798	-16,7473
Electrostatics	-2,00537	-1,93968	-1,6167	0,20407	-1,08109	-0,52361	-2,43496	2,03709	-1,31515
SolvationPolar	17,7702	21,7478	21,1444	21,1689	22,456	36,6253	30,306	36,1728	27,9908
SolvationHydrophobic	-15,8938	-17,5192	-17,9431	-16,3451	-16,1214	-21,4908	-20,5409	-20,0436	-18,7147
Vander Waalsclashes	0,69758	3,79372	1,7873	30,14	0,31265	77,1691	2,78909	84,7845	1,41123
entropysidechain	6,82574	10,471	7,77305	5,79006	6,60429	10,7898	8,94401	9,47957	10,5625
entropymainchain	2,41072	3,66437	5,4694	5,11092	4,52485	7,82553	3,29406	7,0708	6,50957
torsionalclash	0,28695	0,06411	0,94515	1,03191	0,23954	0,41360	0,39516	0,20175	0,06424
backboneclash	3,76599	2,06447	3,27454	4,84797	3,33646	4,73668	3,86164	6,32E+00	3,70501
helixdipole	-0,0515	-0,00195	0	0,0584	-0,01726	0	-0,01829	1,40E-01	-0,29465

electrostatickon	-0,19844	-0,27087	-0,29802	0,03001	-0,28173	-0,15522	-0,28670	0,14051	-0,06865
energylonisation	0,03919	0,05490	0	0	0	0	0	0	0
Entropy Complex	2,384	2,384	2,384	2,384	2,384	2,384	2,384	2,384	2,384
NumberofResidues	778	794	625	630	630	625	625	630	630
Interface Residues	42	44	41	41	44	49	49	49	49
Interface ResiduesClashing	0	0	0	7	0	11	0	16	0
Interface ResiduesVdWClashing	0	0	0	7	0	11	0	16	0
Interface ResiduesBBClashing	0	0	0	1	0	0	0	1	0

Tab. 4 Energy calculations on crystallized structures or 3D comparative models of the investigated protein complex. The PDB.Chain indicates the chain of the PDB used within the indicated analyses on the cited crystallized structures or models obtained by superimposition with the indicated chains. The longest chains were chosen for the "interaction energy" analyses for those crystallized structures with multiple chains. Chain E, F, and S indicate the RBD chain within the investigated PDB_IDs. Chain A and B indicate the ACE2 chain within the investigated PDB_IDs. Chain H, L indicate the heavy and light chain of the investigated antibody (wild type and engineered variants), according to the indicated PDB_ID. PreMin and PostMin refer to models prior and after energy minimization performed on the Yasara minimization server.

DISCUSSION

The indicated pipeline has allowed to set-up a molecular framework hosting SARS-CoV-2 spike protein, ACE2 receptor and different antibodies in the same pdb session that could be handled with different molecular visualizers. In this molecular framework it is possible to study and predict, at molecular level, interactions between the different “pieces” of the framework that my help in understanding virus invasion mechanisms, developing new vaccines or antibodies, identifying small molecules with high affinity for viral proteins and establishing quick/safe diagnosis selective/specific kits. Indeed, the scientific community is now focused in the development of new weapons for containing SARS-CoV-2 spread and COVID-19 complications as it could be observed in the enormous effort in developing new vaccines based on a virus protein/nucleic acid portion able to induce an efficient and specific immunogenic response(56–60), or in developing a neutralizing antibody highly specific for SARS-CoV-2 spike RBD (25, 26, 61–64), or in identifying chemicals with high affinity for SARS-CoV-2 crucial proteins (1–3, 65–67).

Within the presented molecular framework, we have highlighted a set of possible efficient interactions between the crystallized m396 antibody and SARS-CoV-2 spike RBD, raising the question about the possibility to test directly m396 on cultured cells exposed to the virus and then, hopefully, on patients.

Starting from that observation we have also proposed a set of modifications of m396 CDR residues resulting in a higher specific antibody, to be expressed and tested on cultured cells. Along the development of our antibody engineering modeling session an important paper was published and another is under revision in support of the hypothesis that m396 may be able to bind SARS-CoV-2 spike protein (61, 62)**.**

It was also possible to pose in the proposed molecular framework the recent proposed SARS-CoV-2 spike RBD directed CR3022 FAB antibody (6yla.pdb; 6w41.pdb, (62)), showing that it binds a different site of RBD that protrudes towards the central cavity of the spike protein trimer (data not shown). It appears that the RBD-antibody interaction is possible only if at least two RBDs on the trimeric spike protein are in the "open" state of the prefusion conformation and slightly rotated, in a site distant from ACE2 receptor binding region, according to what proposed by the authors (62). Dedicated studies are necessary for understanding if steric hindering problems might rise by using the whole antibody, and deepening the comprehension of the not competitive mechanism that would be observed between CR3022 and RBD in presence of ACE2 receptor.

Studying all the cited interactions in the same pdb-molecular session has allowed to highlight maybe the most crucial ACE2 portions involved in direct interactions with SARS-CoV-2 RBD, suggesting that the administration of the recombinant RBD, a spike monomer or the entire spike trimer, if correctly folded, might result in the efficient triggering of antibody production from our plasma b-cells, reducing COVID-19 complications (supporting what has been recently proposed (56–60)).

At the same time, the ACE2-RBD interactions estimated in our molecular framework has strengthened the hypothesis to use the recombinant ACE2 for limiting COVID-19 infection complications (according to what recently proposed (68, 69)).

A molecular framework like the ones here proposed will also help in studying the putative role of ACE inhibitors in perturbing ACE2-RBD interactions. Indeed, it was recently proposed that patients treated with ACE inhibitors might be more exposed to SARS-CoV-2 infection (70). Although ACE1 (refseq accession number: NP_068576.1, representing the main target of ACE inhibitors) and ACE2 (NP_690043.1, testis isoform or NP_000780, somatic isoform, among the most studied isoforms) share the 40 % of identical residues, few uncertain data about ACE inhibitors and a possible greater selectivity for ACE1 versus ACE2, or on their effect on ACE1/2 expression regulation are available in literature (70, 71). From a structural comparison it is observed that the RMSD of the crystallized native ACE2 coordinates (1r42.pdb, (72)) and ACE1 coordinates (1o8a.pdb, (73)) is lower than 2.5 Å.

Notably, the presence of ACE inhibitors captopril and enalaprilat (1uze.pdb,(74); 4c2p.pdb, (75)) and lisinopril (1o86.pdb, (73)) produces an RMSD lower than 0.3 Å in the atomic coordinates of the cited crystallized structures with reference to the native ACE1 (1r42.pdb, (72)).

Conversely, we cannot establish if the slightly higher RMSD observed between the native ACE2 (1r42.pdb) and ACE2 complexed with SARS-CoV-1 spike RBD (0. 41 Å, 2ajf.pdb) and SARS-CoV-2 spike RBD (1.2 Å, 6vw1.pdb) can be attributed exclusively to interactions with SARS-CoV-RBD, because the observed RMSDs are of the same order of magnitude of the experimental resolution of the investigated crystallized structures.

However, also admitting that ACE1 inhibitors at the employed dosage would target ACE2, with the same efficiency observed versus ACE1, the presence of those inhibitors in ACE2 binding cavity should not be able to induce an important conformational change in ACE2, which might favour a greater affinity of ACE2 versus SARS-CoV-2 spike RBD.

Thus, the only mechanism for which, patients treated with ACE inhibitors would be more exposed to SARS-CoV-2, would rely in a positive feedback induced by ACE inhibitors in ACE2 expression. Nevertheless, evidences in support of this hypothesis need to be deepened (71, 76).

In conclusion, the presented analysis highlights the importance to use fold recognition tools along the approach to a drug design problem according to a rational protocol (similar to what previously reported (29, 30, 49)), like the ones presented. Indeed, in this case, fold recognition tools have helped us in identifying crystallized structures of ACE2, SARS-CoV-spike proteins similar to those under investigation. Furthermore, performing structural comparative analysis has allowed to identify a possible good starting point, like the ones represented by m396, already crystallized in complex with SARS-CoV-1 spike RBD, for building the proposed antibodies. The same strategy might be

applied also for future infections by those researchers involved in drawing new antibodies and/or developing new vaccines, i.e. for dealing with future coronaviruses.

To the best of our knowledge the reported SARS-CoV-2 spike protein trimer 3D model is the first model describing a possible conformational change leading to a reliable SARS-CoV-2 spike protein in post fusion conformation. The proposed model, based on the murine CoV spike protein (6b3o.pdb) crystallized in post fusion conformation, will help in understanding the mechanism allowing the virus envelop fusion with host cell plasma membranes, through and following interactions with ACE2.

Furthermore, the provided 3D model in post-fusion conformation according to the crystallized 3D structure of SARS-CoV-2 spike protein in pre-fusion conformation confirms the presence and stability of a sort of channel at the interface of the three monomers that could represent a good target site of a virtual screening of a chemical/drug library aiming to identify a small molecule/peptide with high affinity for a monomer (similarly to what proposed for EK1 peptide (77)), for preventing trimer formation and stabilization, or a small molecule/peptide with high affinity for the trimer, aiming to prevent conformational changes leading to the fusion of the viral envelope with host cell plasma membranes. The screening of a drug library would help in identifying an already approved drug with high affinity for the spike channel, that might be immediately tested on the bed-side, in the context of the drug-repositioning approaches (78, 79).

Notably, the provided molecular framework for investigating/drawing new antibodies based on space-restraints needs, would be used for the set-up of new antibodies based on the available tissue-specific immunoglobulin structures, as the proposed IgG2A (1igt.pdb, (48)) or other specialized antibodies, already optimized for targeting specific cells or receptors (i.e.1hzh.pdb, (80)), also among those that may successfully target the respiratory tract (1r70.pdb, (81) or 2qtj.pdb (82) or 6ue7.pdb (83)), that might be administered even by aerosol (84, 85).

At the same time, already at the preclinical level, the administered vaccines based on the administration of the entire SARS-CoV-2 spike protein ((56–58) or on the administration of the single SARS-CoV-2 spike RBD, will induce the production of specific antibodies that might be sequenced and modelled *in silico*. On this concern, the provided molecular network will help in quantifying interactions between SARS-CoV-2 RBD (also in cases of different RBD variants (86)) and the newly investigated antibodies, i.e.lower the calculated binding energy in the modelled complex, higher the likelihood to have more success with the investigated vaccines/antibodies.

The discovered antibodies with the highest affinity for RBD might also be implemented in a diagnosis kit aiming to the early identification of SARS-CoV-2 in sera, also in asymptomatic people.

Conversely, a new diagnosis kit could also be based on the native RBD or a modified synthetic RBD, with greater affinity for the detected human antibodies directed against SARS-CoV-2 spike RBD

protein, for determining the real number of healthy people already exposed to the virus in the population.

The lacking knowledge about the real number of people exposed to the virus (including asymptomatic people, people with mild symptoms and rescued people that never needed hospitalization or quarantine) is the only important data that we still miss. Without data about the real number of people, exposed to the virus, in the population, coming back to normal life will be extremely slower.

About technical questions. Detailed instructions for the set-up of the shown molecular framework have been provided in the manuscript. Nevertheless, we can also provide free assistance for academic analyses, upon request. We can also provide dedicated technical support for analyses requested by private companies through our BROWSer s.r.l. spin-off (in this case, please, write to info@browser-bioinf.com and to CLP in Cc).

ACKNOWLEDGEMENTS

Authors would like to thank the Italian Association for Mitochondrial Research (www.mitoairm.it), IT resources made available by ReCaS, a project funded by the MIUR (Italian Ministry for Education, University and Re-search) in the “PON Ricerca e Competitività 2007–2013-Azione I-Interventi di ra_orzamentostrutturale” PONa3_00052, Avviso 254/Ric, University of Bari (“Fondi Ateneo ex-60%”2016”; “ProgettoCompetitivo 2018” and “FFABR 2017-2018”). Authors would also like to thank MIUR for having funded the project “Salute, alimentazione, qualità della vita”: individuazione di un set di biomarker dell’apoptosi” for an innovative industrial PhD course—PON RI 2014-2020, CUP H92H18000160006. Authors would also like to thank Angelo Onofrio (Biotechnologist) and Luna Laera (Biotechnologist) for critical reading and/or stimulating discussions.

Supporting Material

PDB_ID	Chain type	Chains	TargetLen	protein name	virus strain/infected organism	Reference
6vsb	Spike glycoprotein	3	1288	Prefusion 2019-nCoV spike glycoprotein	SARS.CoV.2/H.sapiens	(21)
6vw1	ACE2; 2019-nCoV chomeric RBD	2	597 (ACE2) 217 (2019 nCoV Spike RBD)	2019-nCoV chimeric receptor-binding domain complexed with its receptor human ACE2	SARS.CoV.2/H.sapiens	(54)
6lzg	ACE2; SARS-CoV-2 Spike receptor-binding domain	2	597 (ACE2) 229 (2019 nCoV Spike RBD)	2019-nCoV chimeric receptor-binding domain complexed with its receptor human ACE2	SARS.CoV.2/H.sapiens	To be published
6vyb	Spike glycoprotein	3	1281	SARS-CoV-2 spike ectodomain structure (open state)	SARS.CoV.2/H.sapiens	(22)
6vxx	Spike glycoprotein	3	1281	Structure of the SARS-CoV-2 spike glycoprotein (closed state)	SARS.CoV.2/H.sapiens	(22)
6u7k	Spike glycoprotein	3	821 (1399)	Prefusion structure of PEDV spike	Porcine epidemic diarrhear virus strain CV777/Homo sapiens	(87)
6qfy	Spike glycoprotein	2	288	Porcine hemagglutinating encephalomyelitis virus spike protein lectin domain	Porcine hemagglutinating encephalomyelitis virus/Homo sapiens	(88)
6nzk	Spike surface glycoprotein	3	(1322)940	Structural basis for human coronavirus attachment to	Coronavirus OC43/Homo sapiens	(89)

				sialic acid receptors.		
6nb8	S230 antigen-binding (Fab) fragment, heavy/light chain	1; 1	230; 219	anti- SARS-CoV human neutralizing S230 antibody Fab fragment	H. sapiens	(45)
6nb7	Spike glycoprotein; S230 heavy chain; S230 light chain	3; 3; 3	1263; 127; 112	SARS-CoV complex with human neutralizing S230 antibody Fab fragment (state 2)	SARS.CoV.1/H.sapiens	(45)
6nb6	Spike glycoprotein; S230 heavy/light chain	3; 2; 2	1263; 127; 112	SARS-CoV complex with human neutralizing S230 antibody Fab fragment (state 1)	SARS.CoV.1/H.sapiens	(45)
6nb5	LCA60 antigen-binding (Fab) fragment, heavy/light chain	2; 2	230; 215	anti- MERS-CoV human neutralizing LCA60 antibody Fab fragment	H.sapiens	(45)
6nb4	Spike glycoprotein; LCA60 heavy/light chain	3; 1; 1	(1359) 952; 127; 129	MERS-CoV S complex with human neutralizing LCA60 antibody Fab fragment (state 2)	MERS.CoV/H.sapiens	(45)
6nb3	Spike glycoprotein; LCA60 heavy/light chain	3; 2; 2	(1359) 952; 127; 129	MERS-CoV complex with human neutralizing LCA60 antibody Fab fragment (state 1)	MERS.CoV/H.sapiens	(45)
6m18	Sodium-dependent neutral amino acid transporter		654; 814	ACE2-B0AT1 complex	H.sapiens	(23)

	B(0)AT1; ACE2					
6iex	MHC class I antigen; beta-2-microglobulin	1; 1; 1	274; 100; 10	Crystal structure of HLA-B*4001 in complex with SARS-CoV derived peptide N216-225 GETALALLLL	H.sapiens/H.sapiens/SARS.CoV.1	To be published
6cs2	SARS Spike Glycoprotein - human ACE2 complex	3; 1	1215; 605	Spike glycoprotein,Fibritin; ACE2	SARS.CoV.1/H.sapiens	(42)
6crv	SARS Spike Glycoprotein, Stabilized variant	3	1236;	Spike glycoprotein,Fibritin; ACE2	SARS.CoV.1/H.sapiens	(42)
6c6z	neutralizing antibody CDC2-C2 in complex with MERS-CoV S1 RBD	2; 2; 2	231; 239; 218	Spike glycoprotein; antibody CDC2-C2 heavy/light chain	MERS.CoV./H.sapiens	(90)
6b7n	porcine delta coronavirus spike protein in the pre-fusion state	3	(1107) 948	Spike protein	Delatacoronavirus	(87)
6b30	coronavirus spike glycoprotein in the post fusion state	3	604	Spike glycoprotein	Coronavirus/M.musculus	(37)
6ack	Trypsin-cleaved and low pH-treated SARS-CoV spike glycoprotein and ACE2 complex	3; 1	1203;603	Spike glycoprotein; ACE2	SARS.CoV.1/H.sapiens	(41)

6acj	Cryo-EM structure of the SARS coronavirus spike glycoprotein in complex with its host cell receptor ACE2.	3; 1	1203; 603	Spike glycoprotein; ACE2	SARS.CoV.1/H.sapiens	(41)
6acc	Trypsin-cleaved and low pH-treated SARS-CoV spike glycoprotein and ACE2 complex, ACE2-free conformation with three RBD in down conformation	3	1203	Spike glycoprotein	SARS.CoV.1/H.sapiens	(41)
6acd	Trypsin-cleaved and low pH-treated SARS-CoV spike glycoprotein and ACE2 complex, ACE2-free conformation with one RBD in up conformation	3	1203	Spike glycoprotein	SARS.CoV.1/H.sapiens	(41)
6acg	Trypsin-cleaved and low pH-treated SARS-CoV spike glycoprotein and ACE2 complex, ACE2-bound	3	1203	Splike glycoprotein	SARS.CoV.1/H.sapiens	(41)

	conformation 1					
5zuv	pan-coronavirus fusion inhibitor targeting the HR1 domain of human coronavirus spike.	3	130	Spike glycoprotein,inhibitor EK1		(77)
5zvk	pan-coronavirus fusion inhibitor targeting the HR1 domain of human coronavirus spike.	3; 3	80; 44	Spike glycoprotein HR1 motif; pan-CoV inhibitory peptide EK1	MERS.CoV.1	(77)
5zvm	Pan-coronavirus fusion inhibitor targeting the HR1 domain of human coronavirus spike.	3; 3	80; 44	Spike glycoprotein; pan-CoV inhibitory peptide EK1	SARS.CoV.1	(77)
5yl9	Human Coronavirus 229E fusion core	1; 1	89	Post-fusion core of the Human coronavirus 229E spike protein	SARS.CoV.1	(38)
5xgr	Bat-CoV HKU5	8	(204)198	S1 subunit C-terminal domain from bat-derived coronavirus HKU5 spike protein	Bat-CoV HKU5	(91)
5x58	Prefusion structure of SARS-CoV spike glycoprotein, conformation 1	3	(1228)949	MERS-CoV and SARS-CoV spike glycoproteins	SARS.CoV.1/H. sapiens	(92)

5x4s	N-terminal domain (NTD)of SARS-CoV spike protein	1	(285) 269	Spike glycoprotein	SARS.CoV.1/ H. sapiens	(92)
5x4r	N-terminal domain (NTD) of MERS-CoV spike protein	1	(342) 333	Spike protein	SARS.CoV.1/ H. sapiens	(92)
5szs	Glycan shield and epitope masking of a coronavirus spike protein observed by cryo-electron microscopy	3	(1325) 953	Spike protein	CoV NL63/H. sapiens	(93)
5kwb	Receptor Binding Domain of the Spike Glycoprotein of Human Betacoronavirus HKU1	1	(371) 364	Receptor binding domain of the spike glycoprotein.	BetaCoV/ H.sapiens	(94)
5gyq	receptor-binding domain of bat-derived coronavirus HKU9 spike protein	1	(176) 169	Receptor binding domain of the spike glycoprotein.	Bat coronavirus HKU9	(95)
4qzv	Bat-derived coronavirus HKU4 in complex with CD26	2	208	Dipeptydil peptidase 4 (CD26); Spike protein S1	Bat-derived coronavirus HKU4	(96)
4l3n	Receptor-binding domain from newly emerged Middle East respiratory	2	(216) 209	Receptor-binding doma MERS spike	Betacoronavirus 2c Jordan-N3/2012 /Homo sapiens	(97)

	syndrome coronavirus					
4h14	Bovine Coronavirus Spike Protein Lectin Domain	1	(290) 287	Spike Lectin Domain	CoV; Homo sapiens	(98)
3r4d	Crystal structure of mouse coronavirus receptor-binding domain complexed with its murine receptor	2; 2	208; (288) 229	CEA-related cell adhesion molecule 1, isoform 1/2S ; Spike glycoprotein	Mus musculus / Murine hepatitis virus	(99)
2ghv	SARS spike protein receptor binding domain	2	(203) 183	Spike protein	SARS CoV /H.sapiens	(100)
2fxp	SARS-Coronavirus HR2 Domain	3	55	Spike glycoprotein	SARS CoV /H.sapiens	(101)
2dd8	SARS-CoV Spike Receptor-Binding Domain Complexed with Neutralizing m396 Antibody	3	245; 213; 202	IGG Heavy chain; IGG Light chain; Spike glycoprotein RBD	SARS.CoV.1 / H. sapiens	(44)
2bez	proteolitically resistant core from the severe acute respiratory syndrome coronavirus S2 fusion protein	2	77	E2 glycoprotein	SARS.CoV.1 / H. sapiens	(102)

2ajf	SARS coronavirus spike receptor-binding domain complexed with ACE2	2; 2	597; 180	ACE2; SARS.CoV.1.Spike RBD	SARS.CoV.1 / H. sapiens	(43)
1wyy	Post-fusion hairpin conformation of the sars coronavirus spike glycoprotein	2	(149) 126	E2 Glycoprotein	SARS.CoV.1 / H. sapiens	(39)
1wdf	structure of MHV spike protein post fusion core	2	(95) 91	E2 Glycoprotein	SARS.CoV.1 / Mus musculus	(40)

Supp. Tab. 1 List of the sampled homologous crystallized structures and specific structural features. The listed proteins were sampled by using the folding recognition tools available on pGenTHREADER (http://bioinf.cs.ucl.ac.uk/psipred/) and i-Tasser (https://zhanglab.ccmb.med.umich.edu/I-TASSER/) webservices. SARS-CoV-2 structure with the cited PDB_IDs are also available through the COVID-19/SARS-CoV-2/Resources available on the PDB at the link: https://www.rcsb.org/news?year=2020&article=5e74d55d2d410731e9944f52.

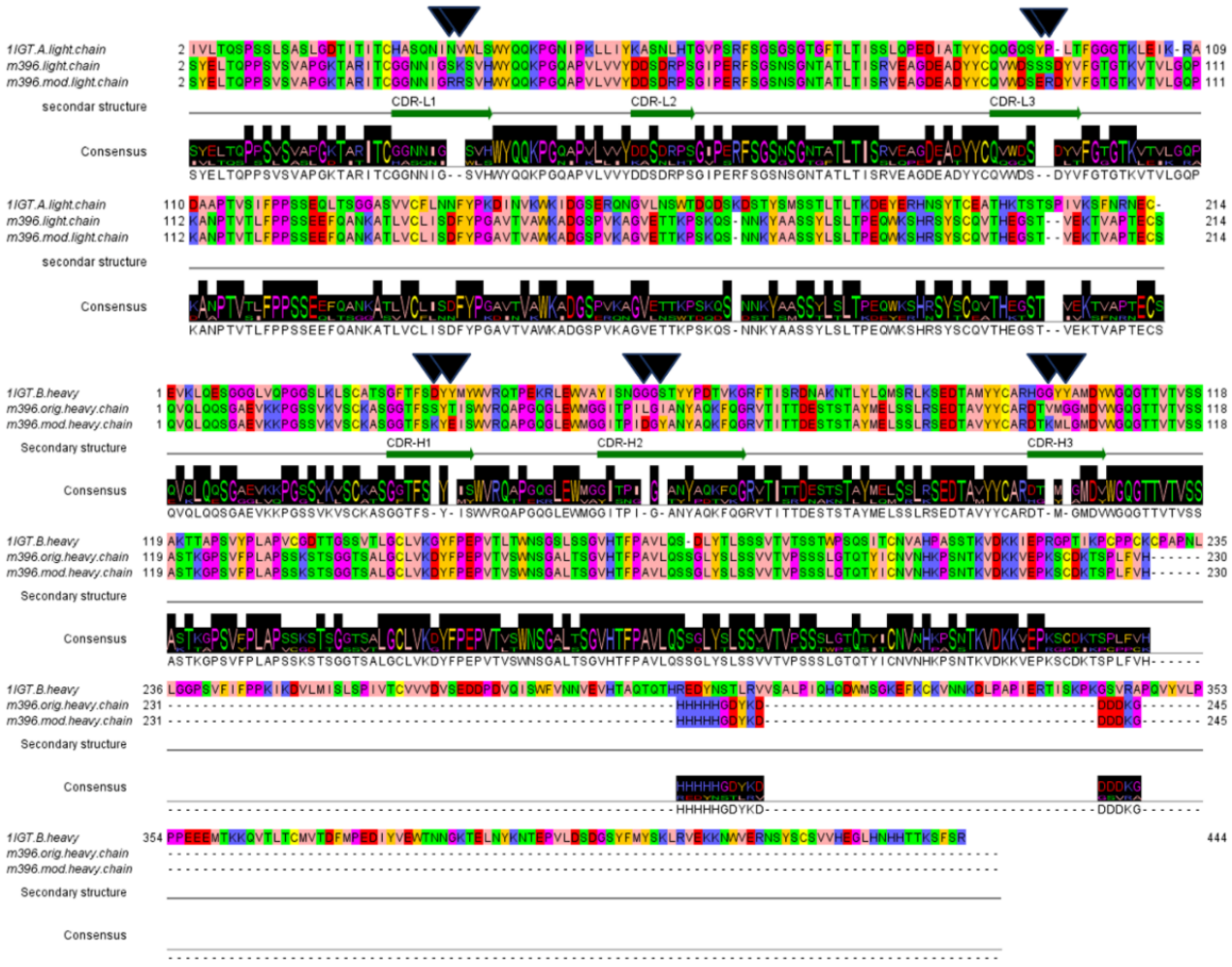

Supp. Fig. 1 MSA of antigen-binding fragment (Fab) of m396 ab (native and modified) with 1IGT.pdb sequece. (A) Pairwise alignment of the light chains from 1IGT (murine IgG) and m396 antibody (native and modified). (B) Pairwise alignment of the heavy chains of the Fab portions from 1IGT and m396 antibody (native and modified.

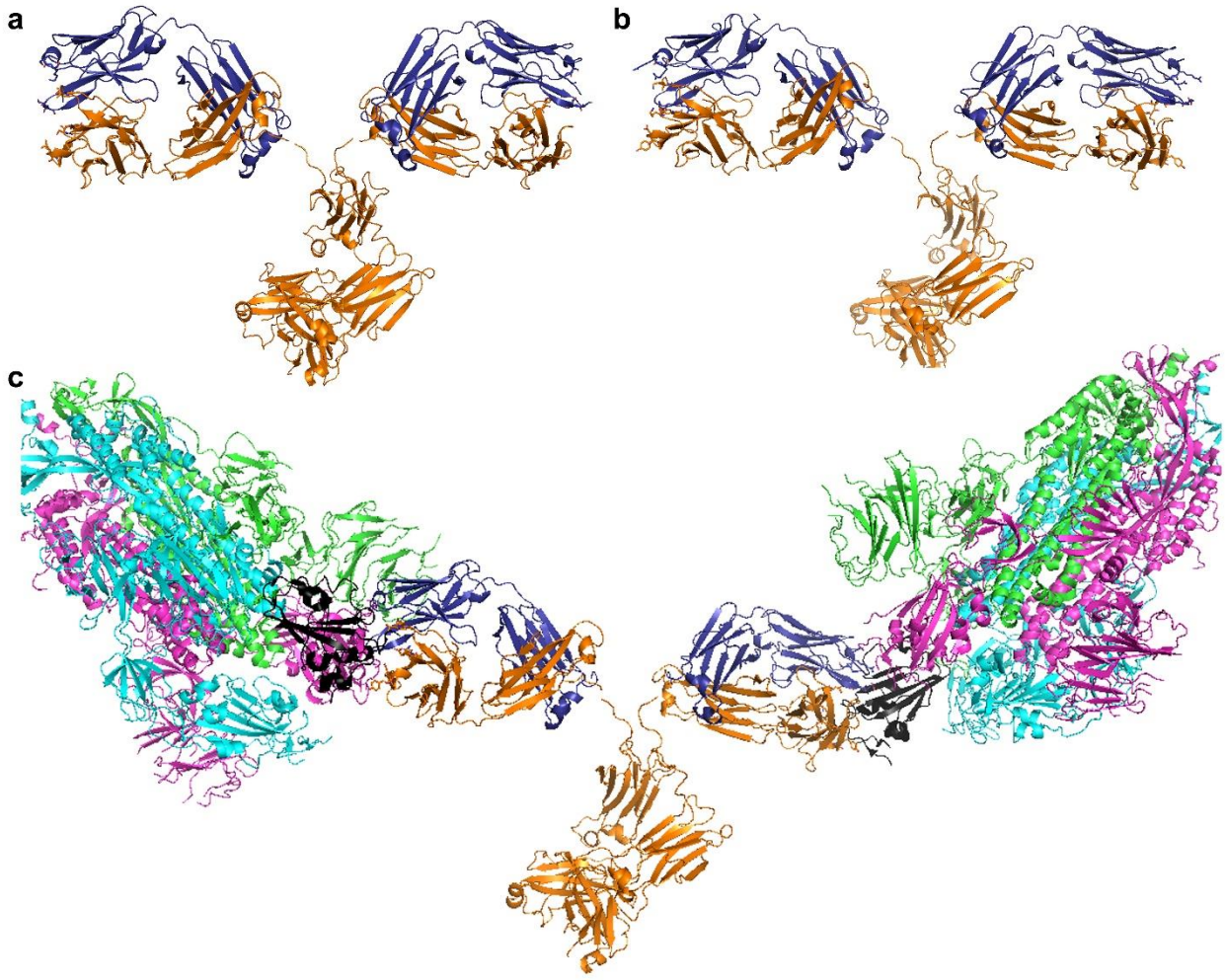

Supp. Fig. 2 The overall structure of 1IGT antibody used as a protein template for building our chimeric mAb models based on m396 ab. The heavy chains are reported in orange cartoons, and the light chains are reported in blue cartoons, for the native m396 (panel a) and for the modified m396 (panel b). SARS-CoV-2 spike proteins are reported in cyan/magenta/green cartoon representation with the exclusion of RBD reported in black cartoon representation. Breaks in the tertiary structures of the antibody backbones (portion in orange cartoon representation), at the interface of the FAB/Fc portion, indicate sites hosting residues that were ligated after superimposition of the different portions (1igt.pdb and native/mutated m396) for obtaining the final complete 3D model of the proposed antibodies.

REFERENCES

1. Gordon, C. J., Tchesnokov, E. P., Feng, J. Y., Porter, D. P., and Gotte, M. (2020) The antiviral compound remdesivir potently inhibits RNA-dependent RNA polymerase from Middle East respiratory syndrome coronavirus. *J. Biol. Chem.* 10.1074/jbc.AC120.013056

2. Elfiky, A. A. (2020) Ribavirin, Remdesivir, Sofosbuvir, Galidesivir, and Tenofovir against SARS-CoV-2 RNA dependent RNA polymerase (RdRp): A molecular docking study. *Life Sci.* https://doi.org/10.1016/j.lfs.2020.117592

3. Wang, M., Cao, R., Zhang, L., Yang, X., Liu, J., Xu, M., Shi, Z., Hu, Z., Zhong, W., and Xiao, G. (2020) Remdesivir and chloroquine effectively inhibit the recently emerged novel coronavirus (2019-nCoV) in vitro. *Cell Res.* 10.1038/s41422-020-0282-0

4. Wu, C., Liu, Y., Yang, Y., Zhang, P., Zhong, W., Wang, Y., Wang, Q., Xu, Y., Li, M., Li, X., Zheng, M., Chen, L., and Li, H. (2020) Analysis of therapeutic targets for SARS-CoV-2 and discovery of potential drugs by computational methods. *Acta Pharm. Sin. B*. 10.1016/j.apsb.2020.02.008

5. Kirchdoerfer, R. N., and Ward, A. B. (2019) Structure of the SARS-CoV nsp12 polymerase bound to nsp7 and nsp8 co-factors. *Nat. Commun.* 10.1038/s41467-019-10280-3

6. Shiraki, K., and Daikoku, T. (2020) Favipiravir, an anti-influenza drug against life-threatening RNA virus infections. *Pharmacol. Ther.* 10.1016/j.pharmthera.2020.107512

7. Hoffmann, M., Kleine-Weber, H., Schroeder, S., Krüger, N., Herrler, T., Erichsen, S., Schiergens, T. S., Herrler, G., Wu, N.-H., Nitsche, A., Müller, M. A., Drosten, C., and Pöhlmann, S. (2020) SARS-CoV-2 Cell Entry Depends on ACE2 and TMPRSS2 and Is Blocked by a Clinically Proven Protease Inhibitor. *Cell*. 10.1016/j.cell.2020.02.052

8. Ton, A.-T., Gentile, F., Hsing, M., Ban, F., and Cherkasov, A. (2020) Rapid Identification of Potential Inhibitors of SARS-CoV-2 Main Protease by Deep Docking of 1.3 Billion Compounds. *Mol. Inform.* 10.1002/minf.202000028

9. Zhang, L., Lin, D., Sun, X., Curth, U., Drosten, C., Sauerhering, L., Becker, S., Rox, K., and Hilgenfeld, R. (2020) Crystal structure of SARS-CoV-2 main protease provides a basis for design of improved α-ketoamide inhibitors. *Science*. 10.1126/science.abb3405

10. Jin, Z., Du, X., Xu, Y., Deng, Y., Liu, M., Zhao, Y., Zhang, B., Li, X., Zhang, L., Peng, C., Duan, Y., Yu, J., Wang, L., Yang, K., Liu, F., Jiang, R., Yang, X., You, T., Liu, X., Yang, X., Bai, F., Liu, H., Liu, X., Guddat, L. W., Xu, W., Xiao, G., Qin, C., Shi, Z., Jiang, H., Rao, Z., and Yang, H. (2020) Structure of Mpro from COVID-19 virus and discovery of its inhibitors. *bioRxiv*. 10.1101/2020.02.26.964882

11. Coutard, B., Valle, C., de Lamballerie, X., Canard, B., Seidah, N. G., and Decroly, E. (2020) The spike glycoprotein of the new coronavirus 2019-nCoV contains a furin-like cleavage site absent in CoV of the same clade. *Antiviral Res.* 10.1016/j.antiviral.2020.104742

12. Tang, N., Bai, H., Chen, X., Gong, J., Li, D., and Sun, Z. (2020) Anticoagulant treatment is associated with decreased mortality in severe coronavirus disease 2019 patients with coagulopathy. *J. Thromb. Haemost.* 10.1111/jth.14817

13. Han, H., Yang, L., Liu, R., Liu, F., Wu, K., Li, J., Liu, X., and Zhu, C. (2020) Prominent changes in blood coagulation of patients with SARS-CoV-2 infection. *Clin. Chem. Lab. Med.* 10.1515/cclm-2020-0188

14. Tang, N., Li, D., Wang, X., and Sun, Z. (2020) Abnormal coagulation parameters are

associated with poor prognosis in patients with novel coronavirus pneumonia. *J. Thromb. Haemost.* 10.1111/jth.14768

15. Yin, S., Huang, M., Li, D., and Tang, N. (2020) Difference of coagulation features between severe pneumonia induced by SARS-CoV2 and non-SARS-CoV2. *J. Thromb. Thrombolysis*. 10.1007/s11239-020-02105-8

16. Mehta, P., Mcauley, D. F., Brown, M., Sanchez, E., Tattersall, R. S., Manson, J. J., Across, H. L. H., and Collaboration, S. (2020) Correspondence COVID-19 : consider cytokine storm syndromes and. *Lancet*. **6736**, 19–20

17. Clerkin, K. J., Fried, J. A., Raikhelkar, J., Sayer, G., Griffin, J. M., Masoumi, A., Jain, S. S., Burkhoff, D., Kumaraiah, D., Rabbani, L., Schwartz, A., and Uriel, N. (2020) Coronavirus Disease 2019 (COVID-19) and Cardiovascular Disease. *Circulation*. 10.1161/CIRCULATIONAHA.120.046941

18. Quagliariello, V., Passariello, M., Coppola, C., Rea, D., Barbieri, A., Scherillo, M., Monti, M. G., Iaffaioli, R. V., De Laurentiis, M., Ascierto, P. A., Botti, G., De Lorenzo, C., and Maurea, N. (2019) Cardiotoxicity and pro-inflammatory effects of the immune checkpoint inhibitor Pembrolizumab associated to Trastuzumab. *Int. J. Cardiol.* **292**, 171–179

19. Colson, P., Rolain, J. M., Lagier, J. C., Brouqui, P., and Raoult, D. (2020) Chloroquine and hydroxychloroquine as available weapons to fight COVID-19. *Int. J. Antimicrob. Agents*. 10.1016/j.ijantimicag.2020.105932

20. Sodhi, M., and Etminan, M. (2020) Safety of Ibuprofen in Patients with COVID-19; Causal or Confounded? *Chest*. 10.1016/j.chest.2020.03.040

21. Wrapp, D., Wang, N., Corbett, K. S., Goldsmith, J. A., Hsieh, C.-L., Abiona, O., Graham, B. S., and McLellan, J. S. (2020) Cryo-EM structure of the 2019-nCoV spike in the prefusion conformation. *Science*. 10.1126/science.abb2507

22. Walls, A. C., Park, Y.-J., Tortorici, M. A., Wall, A., McGuire, A. T., and Veesler, D. (2020) Structure, Function, and Antigenicity of the SARS-CoV-2 Spike Glycoprotein. *Cell*. 10.1016/j.cell.2020.02.058

23. Yan, R., Zhang, Y., Li, Y., Xia, L., Guo, Y., and Zhou, Q. (2020) Structural basis for the recognition of the SARS-CoV-2 by full-length human ACE2. *Science*. 10.1126/science.abb2762

24. Lei, C., Fu, W., Qian, K., Li, T., Zhang, S., Ding, M., and Hu, S. (2020) Potent neutralization of 2019 novel coronavirus by recombinant ACE2-Ig. *bioRxiv*. 10.1101/2020.02.01.929976

25. Wang, Chunyan, Wentao Li, Dubravka Drabekb, Nisreen M.A. Okba, Rien van Haperen,

Albert D.M.E. Osterhaus, Frank J.M. van Kuppeveld, B. L. H., and Frank Grosveld and Berend-Jan Boscha (2020) A human monoclonal antibody blocking SARS-CoV-2 infection Running Head: A cross-neutralizing human antibody targeting SARS-CoV and SARS- CoV-2 Chunyan Wang. *bioRxiv 10.1101/2020.03.11.987958v1*

26. Park, T., Lee, S.-Y., Kim, S., Kim, M. J., Kim, H. G., Jun, S., Kim, S. Il, Kim, B. T., Park, E. C., and Park, D. (2020) Spike protein binding prediction with neutralizing antibodies of SARS-CoV-2. *bioRxiv*. 10.1101/2020.02.22.951178

27. Lobley, A., Sadowski, M. I., and Jones, D. T. (2009) pGenTHREADER and pDomTHREADER: new methods for improved protein fold recognition and superfamily discrimination. *Bioinformatics*. **25**, 1761–1767

28. Yang, J., and Zhang, Y. (2015) Protein Structure and Function Prediction Using I-TASSER. *Curr Protoc Bioinforma.* **52**, 5.8.1-15

29. Trisolini, L., Gambacorta, N., Gorgoglione, R., Montaruli, M., Laera, L., Colella, F., Volpicella, M., De Grassi, A., and Pierri, C. L. (2019) FAD/NADH Dependent Oxidoreductases: From Different Amino Acid Sequences to Similar Protein Shapes for Playing an Ancient Function. *J. Clin. Med.* **8**, 2117

30. Pierri, C. L., Parisi, G., and Porcelli, V. (2010) Computational approaches for protein function prediction: A combined strategy from multiple sequence alignment to molecular docking-based virtual screening. *Biochim. Biophys. Acta - Proteins Proteomics*. 10.1016/j.bbapap.2010.04.008

31. Persson, B. (2000) Bioinformatics in protein analysis. *EXS*. **88**, 215–231

32. Waterhouse, A. M., Procter, J. B., Martin, D. M., Clamp, M., and Barton, G. J. (2009) Jalview Version 2--a multiple sequence alignment editor and analysis workbench. *Bioinformatics*. **25**, 1189–1191

33. Ordog, R. (2008) PyDeT, a PyMOL plug-in for visualizing geometric concepts around proteins. *Bioinformation*. **2**, 346–347

34. Pierri, C. L., Bossis, F., Punzi, G., De Grassi, A., Cetrone, M., Parisi, G., and Tricarico, D. (2016) Molecular modeling of antibodies for the treatment of TNFα-related immunological diseases. *Pharmacol. Res. Perspect.* 10.1002/prp2.197

35. Krieger, E., Joo, K., Lee, J., Lee, J., Raman, S., Thompson, J., Tyka, M., Baker, D., and Karplus, K. (2009) Improving physical realism, stereochemistry, and side-chain accuracy in homology modeling: Four approaches that performed well in CASP8. *Proteins Struct. Funct. Bioinforma.* 10.1002/prot.22570

36. Sanchez, R., Sali, A., Sánchez, R., and Sali, A. (2000) Comparative protein structure modeling. Introduction and practical examples with modeller. *Methods Mol Biol*. **143**, 97–129

37. Walls, A. C., Tortorici, M. A., Snijder, J., Xiong, X., Bosch, B. J., Rey, F. A., and Veesler, D. (2017) Tectonic conformational changes of a coronavirus spike glycoprotein promote membrane fusion. *Proc. Natl. Acad. Sci. U. S. A.* 10.1073/pnas.1708727114

38. Yan, L., Meng, B., Xiang, J., Wilson, I. A., and Yang, B. (2018) Crystal structure of the post-fusion core of the Human coronavirus 229E spike protein at 1.86 Å resolution. *Acta Crystallogr. Sect. D Struct. Biol.* 10.1107/S2059798318008318

39. Duquerroy, S., Vigouroux, A., Rottier, P. J. M., Rey, F. A., and Jan Bosch, B. (2005) Central ions and lateral asparagine/glutamine zippers stabilize the post-fusion hairpin conformation of the SARS coronavirus spike glycoprotein. *Virology*. 10.1016/j.virol.2005.02.022

40. Xu, Y., Liu, Y., Lou, Z., Qin, L., Li, X., Bai, Z., Pang, H., Tien, P., Gao, G. F., and Rao, Z. (2004) Structural basis for coronavirus-mediated membrane fusion: Crystal structure of mouse hepatitis virus spike protein fusion core. *J. Biol. Chem.* 10.1074/jbc.M403760200

41. Song, W., Gui, M., Wang, X., and Xiang, Y. (2018) Cryo-EM structure of the SARS coronavirus spike glycoprotein in complex with its host cell receptor ACE2. *PLoS Pathog.* 10.1371/journal.ppat.1007236

42. Kirchdoerfer, R. N., Wang, N., Pallesen, J., Wrapp, D., Turner, H. L., Cottrell, C. A., Corbett, K. S., Graham, B. S., McLellan, J. S., and Ward, A. B. (2018) Stabilized coronavirus spikes are resistant to conformational changes induced by receptor recognition or proteolysis. *Sci. Rep.* 10.1038/s41598-018-34171-7

43. Li, F., Li, W., Farzan, M., and Harrison, S. C. (2005) Structural biology: Structure of SARS coronavirus spike receptor-binding domain complexed with receptor. *Science (80-.).* 10.1126/science.1116480

44. Prabakaran, P., Gan, J., Feng, Y., Zhu, Z., Choudhry, V., Xiao, X., Ji, X., and Dimitrov, D. S. (2006) Structure of severe acute respiratory syndrome coronavirus receptor-binding domain complexed with neutralizing antibody. *J. Biol. Chem.* 10.1074/jbc.M600697200

45. Walls, A. C., Xiong, X., Park, Y. J., Tortorici, M. A., Snijder, J., Quispe, J., Cameroni, E., Gopal, R., Dai, M., Lanzavecchia, A., Zambon, M., Rey, F. A., Corti, D., and Veesler, D. (2019) Unexpected Receptor Functional Mimicry Elucidates Activation of Coronavirus Fusion. *Cell*. 10.1016/j.cell.2018.12.028

46. Guex, N., Schwede, T., and Peitsch, M. C. (2001) Protein tertiary structure modeling. *Curr Protoc Protein Sci*. **Chapter 2**, Unit2.8

47. DeLano, W. L. (2002) The PyMOL Molecular Graphics System, Version 1.1. *Schr{ö}dinger LLC*. 10.1038/hr.2014.17

48. Harris, L. J., Larson, S. B., Hasel, K. W., and McPherson, A. (1997) Refined structure of an intact IgG2a monoclonal antibody. *Biochemistry*. **36**, 1581–1597

49. Pierri, C. L., Bossis, F., Punzi, G., De Grassi, A., Cetrone, M., Parisi, G., and Tricarico, D. (2016) Molecular modeling of antibodies for the treatment of TNFα-related immunological diseases. *Pharmacol Res Perspect*. **4**, e00197

50. Van Durme, J., Delgado, J., Stricher, F., Serrano, L., Schymkowitz, J., and Rousseau, F. (2011) A graphical interface for the FoldX forcefield. *Bioinformatics*. **27**, 1711–1712

51. Schymkowitz, J., Borg, J., Stricher, F., Nys, R., Rousseau, F., and Serrano, L. (2005) The FoldX web server: an online force field. *Nucleic Acids Res.* **33**, W382-8

52. Deshotels, M. R., Xia, H., Sriramula, S., Lazartigues, E., and Filipeanu, C. M. (2014) Angiotensin II mediates angiotensin converting enzyme type 2 internalization and degradation through an Angiotensin II type I receptor-dependent mechanism. *Hypertension*. 10.1161/HYPERTENSIONAHA.114.03743

53. Wan, Y., Shang, J., Graham, R., Baric, R. S., and Li, F. (2020) Receptor Recognition by the Novel Coronavirus from Wuhan: an Analysis Based on Decade-Long Structural Studies of SARS Coronavirus. *J. Virol.* 10.1128/jvi.00127-20

54. Shang, J., Ye, G., Shi, K., Wan, Y., Luo, C., Aihara, H., Geng, Q., Auerbach, A., and Li, F. (2020) Structural basis of receptor recognition by SARS-CoV-2. *Nature*. 10.1038/s41586-020-2179-y

55. Martin, A. C. R., and Thornton, J. M. (1996) Structural families in loops of homologous proteins: Automatic classification, modelling and application to antibodies. *J. Mol. Biol.* 10.1006/jmbi.1996.0617

56. Chen, W. H., Strych, U., Hotez, P. J., and Bottazzi, M. E. (2020) The SARS-CoV-2 Vaccine Pipeline: an Overview. *Curr. Trop. Med. Reports*. 10.1007/s40475-020-00201-6

57. Kim, E., Erdos, G., Huang, S., Kenniston, T. W., Balmert, S. C., Donahue, C., Raj, V. S., Epperly, M. W., Klimstra, W. B., Haagmans, B. L., Korkmaz, E., Falo, L. D., and Gambotto, A. (2020) Microneedle array delivered recombinant coronavirus vaccines : Immunogenicity and rapid translational development. *EBioMedicine*. **000**, 102743

58. Ahmed, S. F., Quadeer, A. A., and McKay, M. R. (2020) Preliminary identification of potential vaccine targets for the COVID-19 Coronavirus (SARS-CoV-2) Based on SARS-CoV Immunological Studies. *Viruses*. 10.3390/v12030254

59. Thevarajan, I., Nguyen, T. H. O., Koutsakos, M., Druce, J., Caly, L., van de Sandt, C. E., Jia, X., Nicholson, S., Catton, M., Cowie, B., Tong, S. Y. C., Lewin, S. R., and Kedzierska, K. (2020) Breadth of concomitant immune responses prior to patient recovery: a case report of non-severe COVID-19. *Nat. Med.* 10.1038/s41591-020-0819-2

60. Lurie, N., Saville, M., Hatchett, R., and Halton, J. (2020) Developing Covid-19 Vaccines at Pandemic Speed. *N. Engl. J. Med.* 10.1056/NEJMp2005630

61. M. Gordon Joyce, Rajeshwer S. Sankhala, Wei-Hung Chen, Misook Choe, Hongjun Bai, Agnes Hajduczki, Lianying Yan, Spencer L. Sterling, Caroline E. Peterson, Ethan C. Green, Clayton Smith, Natalia de Val, Mihret Amare, Paul Scott, Eric D. Laing, Christopher, K. M. (2020) A Cryptic Site of Vulnerability on the Receptor Binding Domain of the SARS-CoV-2 Spike Glycoprotein. *bioRxiv 10.1101/2020.03.15.992883v1*

62. Yuan, M., Wu, N. C., Zhu, X., Lee, C. D., So, R. T. Y., Lv, H., Mok, C. K. P., and Wilson, I. A. (2020) A highly conserved cryptic epitope in the receptor-binding domains of SARS-CoV-2 and SARS-CoV. *Science (80-.).* **7269**, eabb7269

63. Bhattacharya, M., Sharma, A. R., Patra, P., Ghosh, P., Sharma, G., Patra, B. C., Lee, S. S., and Chakraborty, C. (2020) Development of epitope-based peptide vaccine against novel coronavirus 2019 (SARS-COV-2): Immunoinformatics approach. *J. Med. Virol.* 10.1002/jmv.25736

64. Amanat, F., Nguyen, T., Chromikova, V., Strohmeier, S., Stadlbauer, D., Javier, A., Jiang, K., Asthagiri-Arunkumar, G., Polanco, J., Bermudez-Gonzalez, M., Caplivski, D., Cheng, A., Kedzierska, K., Vapalahti, O., Hepojoki, J., Simon, V., and Krammer, F. (2020) A serological assay to detect SARS-CoV-2 seroconversion in humans. *medRxiv*. 10.1101/2020.03.17.20037713

65. Caly, L., Druce, J. D., Catton, M. G., Jans, D. A., and Wagstaff, K. M. (2020) The FDA-approved Drug Ivermectin inhibits the replication of SARS-CoV-2 in vitro. *Antiviral Res.* 10.1016/j.antiviral.2020.104787

66. Zhou, Y., Hou, Y., Shen, J., Huang, Y., Martin, W., and Cheng, F. (2020) Network-based drug repurposing for novel coronavirus 2019-nCoV/SARS-CoV-2. *Cell Discov.* 10.1038/s41421-020-0153-3

67. Gordon, D. E., Jang, G. M., Bouhaddou, M., Xu, J., Obernier, K., O'Meara, M. J., Guo, J. Z., Swaney, D. L., Tummino, T. A., Huettenhain, R., Kaake, R., Richards, A. L., Tutuncuoglu, B., Foussard, H., Batra, J., Haas, K., Modak, M., Kim, M., Haas, P., Polacco, B. J., Braberg, H., Fabius, J. M., Eckhardt, M., Soucheray, M., Bennett, M. J., Cakir, M., McGregor, M. J., Li, Q., Naing, Z. Z. C., Zhou, Y., Peng, S., Kirby, I. T., Melnyk, J. E., Chorba, J. S., Lou, K.,

Dai, S. A., Shen, W., Shi, Y., Zhang, Z., Barrio-Hernandez, I., Memon, D., Hernandez-Armenta, C., Mathy, C. J. P., Perica, T., Pilla, K. B., Ganesan, S. J., Saltzberg, D. J., Ramachandran, R., Liu, X., Rosenthal, S. B., Calviello, L., Venkataramanan, S., Liboy-Lugo, J., Lin, Y., Wankowicz, S. A., Bohn, M., Sharp, P. P., Trenker, R., Young, J. M., Cavero, D. A., Hiatt, J., Roth, T. L., Rathore, U., Subramanian, A., Noack, J., Hubert, M., Roesch, F., Vallet, T., Meyer, B., White, K. M., Miorin, L., Rosenberg, O. S., Verba, K. A., Agard, D., Ott, M., Emerman, M., Ruggero, D., García-Sastre, A., Jura, N., Zastrow, M. von, Taunton, J., Schwartz, O., Vignuzzi, M., d'Enfert, C., Mukherjee, S., Jacobson, M., Malik, H. S., Fujimori, D. G., Ideker, T., Craik, C. S., Floor, S., Fraser, J. S., Gross, J., Sali, A., Kortemme, T., Beltrao, P., Shokat, K., Shoichet, B. K., and Krogan, N. J. (2020) A SARS-CoV-2-Human Protein-Protein Interaction Map Reveals Drug Targets and Potential Drug-Repurposing. *bioRxiv*. 10.1101/2020.03.22.002386

68. Zhang, H., Penninger, J. M., Li, Y., Zhong, N., and Slutsky, A. S. (2020) Angiotensin-converting enzyme 2 (ACE2) as a SARS-CoV-2 receptor: molecular mechanisms and potential therapeutic target. *Intensive Care Med.* 10.1007/s00134-020-05985-9

69. Batlle, D., Wysocki, J., and Satchell, K. (2020) Soluble angiotensin-converting enzyme 2: a potential approach for coronavirus infection therapy? *Clin. Sci. (Lond).* 10.1042/CS20200163

70. Zheng, Y. Y., Ma, Y. T., Zhang, J. Y., and Xie, X. (2020) COVID-19 and the cardiovascular system. *Nat. Rev. Cardiol.* 10.1038/s41569-020-0360-5

71. Kuster, G. M., Pfister, O., Burkard, T., Zhou, Q., Twerenbold, R., Haaf, P., Widmer, A. F., and Osswald, S. (2020) SARS-CoV2: should inhibitors of the renin–angiotensin system be withdrawn in patients with COVID-19? *Eur. Heart J.* 10.1093/eurheartj/ehaa235

72. Towler, P., Staker, B., Prasad, S. G., Menon, S., Tang, J., Parsons, T., Ryan, D., Fisher, M., Williams, D., Dales, N. A., Patane, M. A., and Pantoliano, M. W. (2004) ACE2 X-Ray Structures Reveal a Large Hinge-bending Motion Important for Inhibitor Binding and Catalysis. *J. Biol. Chem.* 10.1074/jbc.M311191200

73. Natesh, R., Schwager, S. L. U., Sturrock, E. D., and Acharya, K. R. (2003) Crystal structure of the human angiotensin-converting enzyme-lisinopril complex. *Nature*. 10.1038/nature01370

74. Natesh, R., Schwager, S. L. U., Evans, H. R., Sturrock, E. D., and Acharya, K. R. (2004) Structural details on the binding of antihypertensive drugs captopril and enalaprilat to human testicular angiotensin I-converting enzyme. *Biochemistry*. 10.1021/bi049480n

75. Yates, C. J., Masuyer, G., Schwager, S. L. U., Akif, M., Sturrock, E. D., and Acharya, K. R.

(2014) Molecular and thermodynamic mechanisms of the chloride-dependent human angiotensin-I-converting enzyme (ACE). *J. Biol. Chem.* 10.1074/jbc.M113.512335

76. Ferrario, C. M., Jessup, J., Chappell, M. C., Averill, D. B., Brosnihan, K. B., Tallant, E. A., Diz, D. I., and Gallagher, P. E. (2005) Effect of angiotensin-converting enzyme inhibition and angiotensin II receptor blockers on cardiac angiotensin-converting enzyme 2. *Circulation*. 10.1161/CIRCULATIONAHA.104.510461

77. Xia, S., Yan, L., Xu, W., Agrawal, A. S., Algaissi, A., Tseng, C. T. K., Wang, Q., Du, L., Tan, W., Wilson, I. A., Jiang, S., Yang, B., and Lu, L. (2019) A pan-coronavirus fusion inhibitor targeting the HR1 domain of human coronavirus spike. *Sci. Adv.* 10.1126/sciadv.aav4580

78. Law, G. L., Tisoncik-Go, J., Korth, M. J., and Katze, M. G. (2013) Drug repurposing: a better approach for infectious disease drug discovery? *Curr. Opin. Immunol.* 10.1016/j.coi.2013.08.004

79. Cheng, F., Desai, R. J., Handy, D. E., Wang, R., Schneeweiss, S., Barabási, A. L., and Loscalzo, J. (2018) Network-based approach to prediction and population-based validation of in silico drug repurposing. *Nat. Commun.* 10.1038/s41467-018-05116-5

80. Saphire, E. O., Parren, P. W., Pantophlet, R., Zwick, M. B., Morris, G. M., Rudd, P. M., Dwek, R. A., Stanfield, R. L., Burton, D. R., and Wilson, I. A. (2001) Crystal structure of a neutralizing human IGG against HIV-1: a template for vaccine design. *Science (80-.).* **293**, 1155–1159

81. Furtado, P. B., Whitty, P. W., Robertson, A., Eaton, J. T., Almogren, A., Kerr, M. A., Woof, J. M., and Perkins, S. J. (2004) Solution structure determination of monomeric human IgA2 by X-ray and neutron scattering, analytical ultracentrifugation and constrained modelling: A comparison with monomeric human IgA1. *J. Mol. Biol.* 10.1016/j.jmb.2004.03.007

82. Bonner, A., Almogren, A., Furtado, P. B., Kerr, M. A., and Perkins, S. J. (2009) The nonplanar secretory IgA2 and near planar secretory IgA1 solution structures rationalize their different mucosal immune responses. *J. Biol. Chem.* 10.1074/jbc.M807529200

83. Kumar, N., Arthur, C. P., Ciferri, C., and Matsumoto, M. L. (2020) Structure of the secretory immunoglobulin A core. *Science (80-.).* 10.1126/science.aaz5807

84. Zeitlin, L., Cone, R. A., and Whaley, K. J. (1999) Using monoclonal antibodies to prevent mucosal transmission of epidemic infectious diseases. *Emerg. Infect. Dis.* 10.3201/eid0501.990107

85. Cerutti, A., Chen, K., and Chorny, A. (2011) Immunoglobulin Responses at the Mucosal Interface. *Annu. Rev. Immunol.* 10.1146/annurev-immunol-031210-101317

86. Chiara, M., Horner, D. S., and Pesole, G. (2020) Comparative genomics suggests limited variability and similar evolutionary patterns between major clades of SARS-Cov-2. *bioRxiv*. 10.1101/2020.03.30.016790

87. Wrapp, D., and McLellan, J. S. (2019) The 3.1-Angstrom Cryo-electron Microscopy Structure of the Porcine Epidemic Diarrhea Virus Spike Protein in the Prefusion Conformation. *J. Virol.* 10.1128/jvi.00923-19

88. Hulswit, R. J. G., Lang, Y., Bakkers, M. J. G., Li, W., Li, Z., Schouten, A., Ophorst, B., Van Kuppeveld, F. J. M., Boons, G. J., Bosch, B. J., Huizinga, E. G., and De Groot, R. J. (2019) Human coronaviruses OC43 and HKU1 bind to 9-O-acetylated sialic acids via a conserved receptor-binding site in spike protein domain A. *Proc. Natl. Acad. Sci. U. S. A.* 10.1073/pnas.1809667116

89. Alejandra Tortorici, M., Walls, A. C., Lang, Y., Wang, C., Li, Z., Koerhuis, D., Boons, G. J., Bosch, B. J., Rey, F. A., de Groot, R. J., and Veesler, D. (2019) Structural basis for human coronavirus attachment to sialic acid receptors. *Nat. Struct. Mol. Biol.* 10.1038/s41594-019-0233-y

90. Wang, L., Shi, W., Chappell, J. D., Joyce, M. G., Zhang, Y., Kanekiyo, M., Becker, M. M., van Doremalen, N., Fischer, R., Wang, N., Corbett, K. S., Choe, M., Mason, R. D., Van Galen, J. G., Zhou, T., Saunders, K. O., Tatti, K. M., Haynes, L. M., Kwong, P. D., Modjarrad, K., Kong, W.-P., McLellan, J. S., Denison, M. R., Munster, V. J., Mascola, J. R., and Graham, B. S. (2018) Importance of Neutralizing Monoclonal Antibodies Targeting Multiple Antigenic Sites on the Middle East Respiratory Syndrome Coronavirus Spike Glycoprotein To Avoid Neutralization Escape. *J. Virol.* 10.1128/jvi.02002-17

91. Han, X., Qi, J., Song, H., Wang, Q., Zhang, Y., Wu, Y., Lu, G., Yuen, K. Y., Shi, Y., and Gao, G. F. (2017) Structure of the S1 subunit C-terminal domain from bat-derived coronavirus HKU5 spike protein. *Virology*. 10.1016/j.virol.2017.04.016

92. Yuan, Y., Cao, D., Zhang, Y., Ma, J., Qi, J., Wang, Q., Lu, G., Wu, Y., Yan, J., Shi, Y., Zhang, X., and Gao, G. F. (2017) Cryo-EM structures of MERS-CoV and SARS-CoV spike glycoproteins reveal the dynamic receptor binding domains. *Nat. Commun.* 10.1038/ncomms15092

93. Walls, A. C., Tortorici, M. A., Frenz, B., Snijder, J., Li, W., Rey, F. A., DiMaio, F., Bosch, B. J., and Veesler, D. (2016) Glycan shield and epitope masking of a coronavirus spike protein observed by cryo-electron microscopy. *Nat. Struct. Mol. Biol.* 10.1038/nsmb.3293

94. Ou, X., Guan, H., Qin, B., Mu, Z., Wojdyla, J. A., Wang, M., Dominguez, S. R., Qian, Z., and Cui, S. (2017) Crystal structure of the receptor binding domain of the spike glycoprotein of

human betacoronavirus HKU1. *Nat. Commun.* 10.1038/ncomms15216

95. Huang, C., Qi, J., Lu, G., Wang, Q., Yuan, Y., Wu, Y., Zhang, Y., Yan, J., and Gao, G. F. (2016) Putative Receptor Binding Domain of Bat-Derived Coronavirus HKU9 Spike Protein: Evolution of Betacoronavirus Receptor Binding Motifs. *Biochemistry*. 10.1021/acs.biochem.6b00790

96. Wang, Q., Qi, J., Yuan, Y., Xuan, Y., Han, P., Wan, Y., Ji, W., Li, Y., Wu, Y., Wang, J., Iwamoto, A., Woo, P. C. Y., Yuen, K. Y., Yan, J., Lu, G., and Gao, G. F. (2014) Bat origins of MERS-CoV supported by bat Coronavirus HKU4 usage of human receptor CD26. *Cell Host Microbe*. 10.1016/j.chom.2014.08.009

97. Chen, Y., Rajashankar, K. R., Yang, Y., Agnihothram, S. S., Liu, C., Lin, Y.-L., Baric, R. S., and Li, F. (2013) Crystal Structure of the Receptor-Binding Domain from Newly Emerged Middle East Respiratory Syndrome Coronavirus. *J. Virol.* 10.1128/jvi.01756-13

98. Peng, G., Xu, L., Lin, Y. L., Chen, L., Pasquarella, J. R., Holmes, K. V., and Li, F. (2012) Crystal structure of bovine coronavirus spike protein lectin domain. *J. Biol. Chem.* 10.1074/jbc.M112.418210

99. Peng, G., Sun, D., Rajashankar, K. R., Qian, Z., Holmes, K. V., and Li, F. (2011) Crystal structure of mouse coronavirus receptor-binding domain complexed with its murine receptor. *Proc. Natl. Acad. Sci. U. S. A.* 10.1073/pnas.1104306108

100. Hwang, W. C., Lin, Y., Santelli, E., Sui, J., Jaroszewski, L., Stec, B., Farzan, M., Marasco, W. A., and Liddington, R. C. (2006) Structural basis of neutralization by a human anti-severe acute respiratory syndrome spike protein antibody, 80R. *J. Biol. Chem.* 10.1074/jbc.M603275200

101. Hakansson-McReynolds, S., Jiang, S., Rong, L., and Caffrey, M. (2006) Solution structure of the severe acute respiratory syndrome-coronavirus heptad repeat 2 domain in the prefusion state. *J. Biol. Chem.* 10.1074/jbc.M601174200

102. Supekar, V. M., Bruckmann, C., Ingallinella, P., Bianchi, E., Pessi, A., and Carfi, A. (2004) Structure of a proteolytically resistant core from the severe acute respiratory syndrome coronavirus S2 fusion protein. *Proc. Natl. Acad. Sci. U. S. A.* 10.1073/pnas.0406128102